MARMARA UNIVERSITY
INSTITUTE FOR GRADUATE STUDIES
IN PURE AND APPLIED SCIENCES

NUMERICAL ANALYSIS AND EXPERIMENTAL VERIFICATION OF INDUSTRIAL LITHIUM-ION BATTERIES

RECEP UYSAL

MASTER THESIS

Department of Mechanical Engineering

Thesis Supervisor

Assoc. Prof. Barış YILMAZ

ISTANBUL, 2022

MARMARA UNIVERSITY
INSTITUTE FOR GRADUATE STUDIES
IN PURE AND APPLIED SCIENCES

NUMERICAL ANALYSIS AND EXPERIMENTAL VERIFICATION OF INDUSTRIAL LITHIUM-ION BATTERIES

RECEP UYSAL

MASTER THESIS

Department of Mechanical Engineering

Thesis Supervisor

Assoc. Prof. Barış YILMAZ

ISTANBUL, 2022

ACKNOWLEDGMENTS

Foremost, I would like to express my sincere gratitude to my advisor Assoc. Prof. Barış Yılmaz, for the continuous support of my thesis, for his patience, motivation, enthusiasm, and immense knowledge. His guidance helped me in all the time of research and writing of this thesis.

I would also like to specially thank my dear wife Seren Uysal, my deceased father Mustafa Uysal and my family, for their infinite support, love and priceless motivation throughout this project and thesis.

Finally, I would like to thank Vestel Company for providing all kinds of equipment, tools and opportunities throughout my thesis. I would also like to thank all my managers, my mechanical R&D colleagues, and the experimental team for their support.

TABLE OF CONTENTS

ÖZET

ENDÜSTRİYEL LİTYUM-İYON PİLLERİN SAYISAL ANALİZİ VE DENEYSEL DOĞRULAMASI

Bu tez kapsamında Li-ion piller ile çalışmalar gerçekleştirilmiştir. Batarya paketleri içerisinde, silindirik ve prizmatik Li-ion piller olmak üzere iki farklı pil kimyasının batarya paketleri içerisindeki davranışları incelenmiştir. Pillerin analizleri ANSYS Fluent ticari yazılımı ile gerçekleştirilmiştir. Sonrasında, deneyler yapılarak pillerin performansları ve termal sonuçları incelenmiştir. Analiz sonuçları ile deney sonuçları karşılaştırılmış ve çalışmaların birbiri ile olan uyumluluğu ortaya koyulmuştur.

Tez çalışması iki gruba ayrılmıştır. İlk olarak, şarjlı bir elektrik süpürgesinde kullanılan batarya modülü yapısı incelenmiştir. Batarya modülü 7 adet LG INR 18650 tipi pillerin seri olarak bağlantı yapılmasıyla elde edilmiştir. Her bir pil 3,63V gerilime ve 12,5 Wh kapasiteye sahiptir. Batarya modülünde ilk olarak HPPC (Hybrid Pulse Power Characterization) deneyleri gerçekleştirilmiştir. HPPC deneyleriyle, farklı ortam sıcaklıklarında ve SOC(State of Charge) değerlerindeki pillerin gerilim değerleri ölçülmüştür. HPPC deneylerinde elde edilen gerilim ve SOC değerleri, ANSYS Fluent Battery Modul analizlerinde kullanılmıştır. Bu analiz aracılığıyla, her pile ait, zamana bağlı ısı üretim değeri çıktıları elde edilmiştir. Elde edilen bu ısı üretim değerleri sonrasında Fluent Termal analizlerde ısı girdisi olarak kullanılmış ve tüm batarya modülü piller ile birlikte modellenmiştir. Bu analizler sayesinde batarya modülünün ısıl davranışı elde edilmiştir.

Tez kapsamında yapılan ikinci çalışma ise, prizmatik piller kullanılarak elde edilen batarya modülünde gerçekleştirilen termal analizler ve deneyler olmuştur. Bu batarya modülü, telekom baz istasyonlarında kullanılmaktadır ve ilk projedeki elektrik süpürgesi batarya modülüne göre daha kapsamlı bir çalışmadır. Önceki projede olduğu gibi analiz ve deney sıralamaları aynı şekilde uygulanmıştır. Bu projede ayrıca batarya iç dirençleri ve akım değerlerine bağlı olarak kapasite hesabı da yapılmıştır. HPPC deneyleri yapılmış, tekil pillere ait çalışma performansları kaydedilmiştir. Sonrasında hesaplanan ısı çıktıları ile termal analizlere geçilmiştir. Termal analizler esnasında tüm batarya modülü analize dahil edilmiştir. Tüm kritik sıcaklık değerleri ve bölgeleri tespit edilmiştir. Ayrıca bu çalışmada, modül içerisinde düşük sıcaklıklarda şarj işlemini gerçekleştirmek için bir ön ısıtıcı ve batarya modülünün deşarjı sırasında elektronik bileşenlerde oluşacak yüksek sıcaklıkları engellemek için pasif soğutma sistemi de tasarlanmıştır.

Her iki proje için de, termal analizler tamamlandıktan sonra kritik sıcaklıklara sahip piller üzerine NTC sensörü yerleştirilerek deney hazırlıkları yapılmıştır. Elektrik süpürgesi batarya modülünde termal deneyler gerçekleştirilmiş ve analiz sonuçları ile karşılaştırılmıştır. Telekom baz istasyonu batarya modülünde ise tüm termal analizler ve soğutma analizleri gerçekleştirilmiş, kritik sıcaklık noktaları ve bölgeler belirlenmiştir. Fakat imalat süreçlerinin yetişmemesi ve parça tedarik süreçlerinin proje süresinde yetişmemesi sebebiyle, termal deneyler yapılamamıştır.

ABSTRACT

NUMERICAL ANALYSIS AND EXPERIMENTAL VERIFICATION OF INDUSTRIAL LITHIUM-ION BATTERIES

Within the scope of this thesis, Li-ion batteries studies were carried out. The behavior of two different battery chemistries in battery packs, cylindrical and prismatic Li-ion batteries, has been investigated. The analyzes of the batteries were performed with ANSYS Fluent commercial software. Afterwards, the performances and thermal results of the batteries were investigated by experiments. The results of the numerical analysis and the experiments were compared and the agreement between the studies was revealed.

The thesis work is divided into two groups. First, the battery module structure in a rechargeable vacuum cleaner was investigated. The battery module is obtained by connecting 7 LG INR 18650 batteries in series. Each battery has a voltage of 3.63V and a capacity of 12.5 Wh. Hybrid Pulse Power Characterization (HPPC) experiments were carried out for the battery module at the beginning. With HPPC experiments, the voltage values of the batteries at different ambient temperatures and State of Charge (SOC) values were measured. Voltage and SOC values obtained in HPPC experiments were used in ANSYS Fluent Battery Module analysis. Through this analysis, time dependent heat generation value outputs of each battery were obtained. After that, Fluent Thermal analyzes were used as heat input and all battery modules were modeled together with the batteries. Thanks to these analyzes, the thermal behavior of the battery module has been obtained.

The second study within the scope of the thesis was the thermal analyzes and experiments carried out on the battery module obtained by using prismatic batteries. This battery module was used in telecom base stations. A more comprehensive study has been carried out than the vacuum cleaner battery module in the first project. As in the previous project, the analysis and experiment sequences were applied in the same way. In this project, the capacity calculation was also made depending on the battery internal resistances and current values. HPPC experiments were carried out and the operating performances of individual batteries were recorded. Afterwards, thermal analyzes were carried out and these calculated heat outputs were used. During the thermal analysis, the entire battery module was included in the analysis. All critical temperature values and zones have been determined. In addition, in this study, a preheater was designed to perform the charging process at low temperatures inside the module,

and a passive cooling system was designed to prevent high temperatures that would occur in the electronic components during the discharge of the battery module.

For both projects, experiments were conducted by locating the NTC sensors on the batteries having critical temperatures after the thermal analysis was completed. Thermal experiments were carried out on the vacuum cleaner battery module and compared with the analysis results. In the telecom base station battery module, all thermal and cooling analyzes were carried out, and critical temperature points and regions were determined. However, thermal experiments could not be performed due to the lack of production processes and parts supply processes within the thesis period.

SYMBOLS

α	: Alpha
Al	: Aluminum
Li	: Lithium
℃	: Celsius
LFP	: Lithium-Iron Phosphate
LCO	: Lithium Cobalt Oxide
LMO	: Lithium-Manganese Oxide
NMC	: Lithium-Manganese Oxide
C-rate	: Charging Rate
In	: Inlet
Out	: Outlet
BC	: Before Christ
AD	: Anno Domini
Zn	: Zinc
Cu	: Copper
V	: Volt
I	: Current
Pb	: Lead
O_2	: Oxygen
H_2	: Hydrogen
S	: Sulphur
e	: Electron
Ni	: Nickel
Cd	: Cadmium
MH	: Metal Hydride
Co	: Cobalt
Mn	: Manganese
R_s, R_1 and R_2	: Resistors' Resistance
C_1 and C_2	: Capacitors' Capacitance

TC	: Thermocouple
ρ	: Density
C_p	: Specific Heat
K	: Kelvin
m	: Meter
mm	: Millimeter
W	: Watt
Ω	: Ohm

ABBREVIATIONS

Ah	: Ampere Hour
BMS	: Battery Management System
BOL	: Beginning of Life
BP	: British Petroleum
BTMS	: Battery Thermal Management System
CFD	: Computational Fluid Dynamic
CHT	: Conjugate Heat Transfer
DOD	: Depth or Discharge
ECM	: Equivalent Circuit Model
EOL	: End of Life
ESS	: Energy Storage System
EV	: Electric Vehicle
HC	: Hydro Carbon
HEV	: Hybrid Electric Vehicle
HPPC	: Hybrid Pulse Power Characterization
MSMD	: Multi Scale Multi Dimension
NTC	: Negative Temperature Coefficient
OCV	: Open Circuit Voltage
PC-ABS	: Polycarbonate/Acrylonitrile Butadiene Styrene
PCB	: Printed Circuit Board
PHEV	: Plug-in Hybrid Electric Vehicle
RUL	: Remaining Useful Lifetime
SOC	: State of Charge
SOH	: State of Health
TBS	: Telecom Base Station

LIST OF FIGURES

LIST OF TABLES

1. INTRODUCTION

Since the beginning of the 21st century, awareness has increased that fossil fuels cause environmental pollution, that this pollution is very harmful to human health, and that waste gases producing from the burning of fossil fuels cause global warming by resulting in a greenhouse effect. Besides these effects, the limited fossil fuel resources will cause the power plants or industries that generate power from these fuels to stop functioning in the future, and this may lead our world into serious crises. In addition, the demand for fossil fuels is increasing rapidly globally in our world, which is developing day by day in every aspect and its needs are increasing. In this context, according to BP Statistical Review of World Energy 2016 and BP Energy Outlook 2016, the fossil fuel needed by our global world has increased by 1.9 million barrels per day, and 2/3 of this increase belongs to the transportation sector [1], [2].

In order to reduce the gases polluting the atmosphere and creating greenhouse effect, energy efficient and environmentally friendly electric vehicles, hybrid vehicles and plug-in hybrid vehicles are promising solutions instead of vehicles with traditional internal combustion engines. Andersen et al., in their study, stated that if the energy to be used by electric vehicles can be obtained from renewable energy sources such as solar or wind, air pollution caused by fossil fuels can be reduced by 40 percent [3].

The rise of renewable energy generation in the current energy market has created enormous potential for different forms of energy storage. Lithium batteries are at the forefront of these storage technologies due to their light weight and high energy density. The properties of lithium batteries have made them attractive for both electronics and automotive applications.

With industrialization and globalization, energy demand has been increasing day by day. Energy storage systems, batteries are important through their ability to store energy during peak hours and give energy during peak hours to ensure consistent energy quality and reasonable use of energy [4].

Today, the importance of batteries is increasing day by day. The widespread use of portable electronic devices (computers, mobile phones, audio and video devices, etc.) has greatly increased the need for batteries. In industrial and commercial applications, the use of battery-backed power systems is becoming increasingly common during utility power outages. The importance of batteries, which provide the first movement to the internal combustion engine and used as accumulators in the automotive industry for many years, is increasing day by day due to the acceleration of the studies on the development of hybrid or fully electric vehicles.

Due to the diversity in usage areas, many different types and features of batteries are produced. Daily or single-use batteries, despite their low power density and capacity, are small in size and have the advantage of portability. In industrial applications, large-volume battery types with high capacity and power density are generally used, and the batteries in this group have the feature of being recharged. Although disposable batteries are mostly preferred for daily use, they are replaced by rechargeable batteries over time.

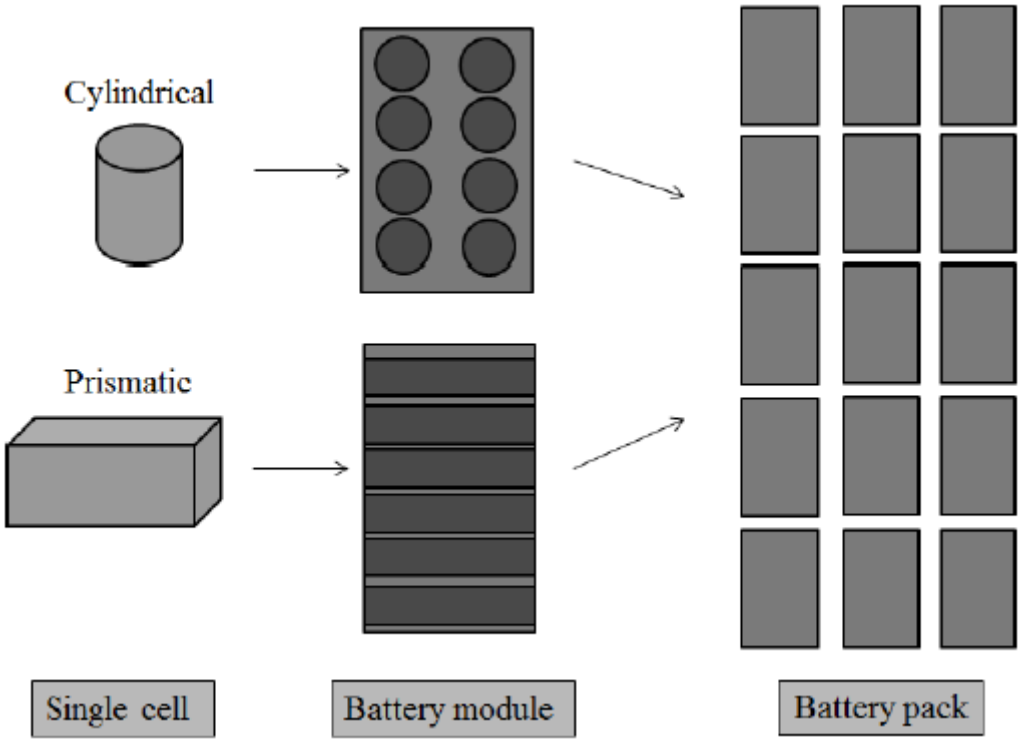

Figure 1.1. Different Battery Geometries [5]

In order for Li-ion cells to become more actively involved in our daily lives and to increase their use, governments provide advantages such as free or cheap pricing, lower transportation taxes and the absence of emission taxes to electric vehicle owners. Many developed country governments have announced that they will have some regulations to limit the production of fuel-based vehicles. Sales and demand for Electric Vehicles (EVs) are increasing day by day, and automotive companies are investing heavily to get their share of the pie.

The main reason why it is not widely accepted by the consumer is that these batteries are expensive, have a limited lifespan, consumer's safety concerns, and deterioration in the battery due to temperature increase. Extreme efforts are being made to find better electrode materials in order to extend the life of the batteries and to produce batteries with higher specific energy and specific power. However, thermal research for the development of battery thermal

management system under various conditions has not been adequately addressed, although temperature conditions have a serious impact on the performance, life and safety of the battery. The acceptable operating temperature range of these batteries ranges from -20 to 60°C [6]. However, in order to maintain its optimum performance, Peseran et al. suggested that it should operate between 15°C and 35°C, which is a slightly narrower range [7]. Exceeding the desired temperature will cause enormous capacity losses in the battery. Motloch et al. showed that each degree increase in the operating temperature between 30°C and 40°C reduces the battery life by approximately 2 months [8]. In addition, in a single battery cell or battery pack, it is desired that the temperature difference should not be more than 5° locally, since it will give positive results in terms of both performance and life [9]. In line with these data, it has become necessary to develop a thermal management system to keep the battery in the optimum temperature range. An effective battery thermal management system is required to dissipate the heat generated inside the batteries. Also, in low temperature scenarios, heating is required to ensure optimal performance.

1.1. Battery Components

1.1.1. Anode

The negative side of the electrode is known as the anode. During the electrochemical reaction, the electrons pass over it and flow in to the electrical circuit, and at the same time, oxidation occurs during the electrochemical reaction [10].

The anode is the negative "-" section in the battery cell. Generally, the conductive material is coated with carbon material, especially graphite. The conductor is a thin piece of aluminum or copper with a high conductivity level.

1.1.2. Cathode

It is the electrode that takes the electrons passing through the electrical circuit. Reduction takes place on this electrode during electrochemical reactions.

The cathode, the working principle is generally the reverse of the anode; The positive "+" section inside the battery cell is called the cathode. Generally, in materials chemistry, it is a thin piece of Aluminum or Copper coated with Lithium Ion chemistry such as Lithium-Iron Phosphate (LFP), Lithium Cobalt Oxide (LCO).

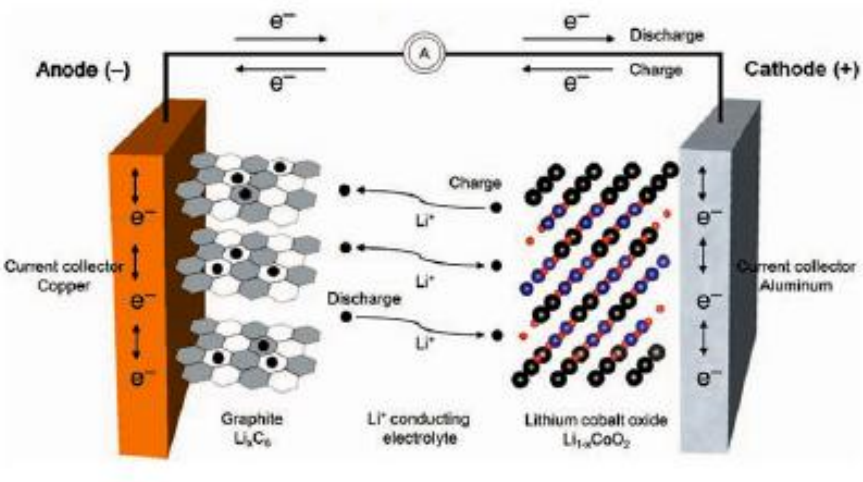

Figure 1.2. Movement of Li+ in an Electrolyte in a Battery [11]

1.1.3. Electrolyte

It provides charge transfer between the anode and cathode in the battery by means of ions and allows the electric current to complete the circuit. Electrolyte is formed by dissolving various salts in water, base or acids or organic solvents. Solid electrolytes are used in some batteries.

1.1.4. Separator

A separator is a thin piece of material, often a plastic or ceramic, which separates the anode from the cathode. The main purpose of the separator is just to separate the anode from the cathode.

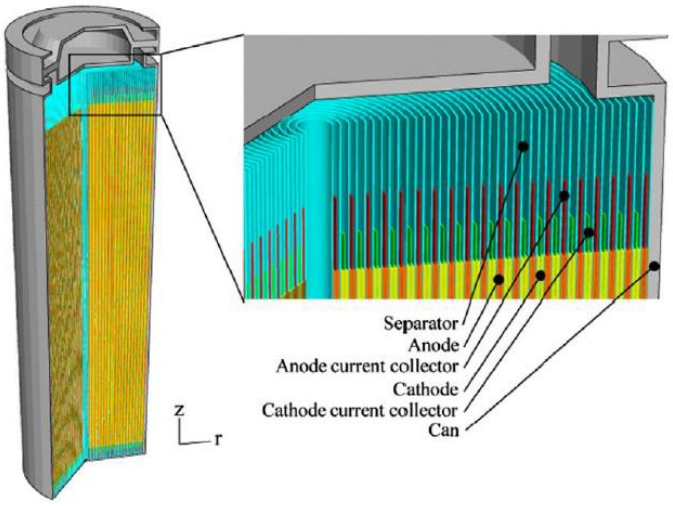

Figure 1.3. Basic Structure of the Lithium-ion Cell [12]

1.2. Li-ion Battery Terms

1.2.1. Battery Management System (BMS)

The BMS communicates with the vehicle system, providing controls in the charging and discharging process, as well as keeping temperature and voltage changes under control. It is a control system in a battery pack, generally consisting of one or more electronic controllers whose cells balance and manage safety and operating performance.

1.2.2. Capacity

The capacity can be defined as, the electrical energy storage capability of a battery in ampere hours (Ah). Capacity can be calculated by drawing a constant current from a fully charged battery until the end-of-discharge voltage is reached. The current times elapsed time will give capacity in Ah. Capacity can be changed due to C-rate, at higher charge/discharge current rates battery capacity is lower. At higher currents, the voltage dissipation tends to be greater; thus, end-of-discharge or end-of-charge voltages reached earlier.

1.2.3. C-rate

The term C-rate is important; it refers to the rate at which a battery can charge or discharge all of its energy (or power). In other words, it describes how fast a battery can accept a charge or give up its power (discharge). C-rate is described in relation to a 1 h discharge, so 1C-rate is equal to the rate at which a battery is fully discharged (or charged) in 1 h. Along the same lines, 2C-rate would then be equal to the rate at which a battery is fully discharged in 30 min (60 min/2C = 30 min). If the C-rate number goes up the discharge time goes down, and vice versa. So 0.5C discharge rate would be equal to a 2 h discharge period.

1.2.4. Depth of Discharge (DOD)

Depth of Discharge (DOD) is a measurement system that determines the utilization rate and amount of cell or packet energy. Generally, only 20% to 90% of the total energy amount is considered appropriate to use a lithium-ion battery.

DOD is another way to keep track of the remaining energy of the battery. Simply, DOD is the measure of the charge removed from a battery in Ah or percentage. If it is expressed in percentage basically, DOD (%) = 100 – State of Charge (SOC) (%). But in literature, it is stated that expressing DOD in Ah is more advantageous. The reason is when all of the charge is removed from the cell the SOC will be 0%, at this point if you were to remove more energy from the cell, the SOC value cannot go lower, only DOD(Ah) can continue to count removed

energy. Same applies for overcharging, the SOC value cannot track values more than 100%, but DOD can be represented in negative values [13].

1.2.5. Open-Circuit Voltages (OCV)

The voltage measured between battery terminals when a current flow over the battery is called terminal voltage. On the other hand, open-circuit voltage (OCV) is the resting voltage of the battery, or steady-state voltage value when no current disturbance is applied to the battery [14].

1.2.6. Energy Storage System (ESS)

The term Energy Storage System (ESS) refers to the completeness of the battery pack and a system that is usually activated during power outages. ESS is a combination of mechanically and electrically coupled cells with appropriate thermal, electronic and mechanical structure within the entire battery pack.

1.2.7. State of Charge (SOC)

SOC shows the amount of change in the capacity of the battery during operation. SOC usually measures between 0% and 100% of capacity.

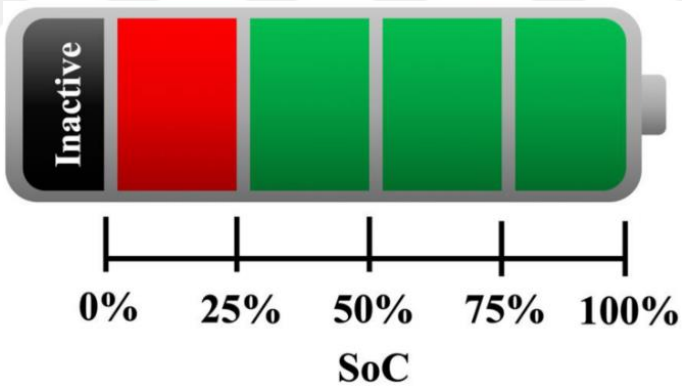

Figure 1.4. Stored Energy Status of a Lithium-Ion Battery Related to State-of-Charge [15]

1.2.8. State of Health (SOH)

During the lifetime of the battery, some irreversible chemical reactions take place resulting capacity to reduce, internal resistance to increase, etc., and the overall performance of the battery will reduce. Hence, an aging measure is needed to be employed in order to estimate the remaining useful lifetime (RUL) of the battery. Although, the SOH is a definition may differ from manufacturer to manufacturer. It can be generalized as an arbitrary measure that allows comparing batteries present conditions with the Beginning of Life (BOL) conditions. Many of the works in literature uses only capacity reduction as the primary indicator of the SOH, but

there is a considerable amount of works that also take account of the increment in internal resistance [16, 17]. Just like operating outside of the suggested working conditions will damage the battery and accelerate aging effects resulting premature aging, some of the reasons can be listed as vicious currents cycles, extreme temperatures, overcharging, under discharging, etc. [18,19].

1.2.9. Cut-off Voltage

This term is used to express extreme voltage points of the battery. A battery should not be discharged below the low cut-off voltage or charged above the high cut-off voltage. Otherwise, irreversible chemical reactions might occur, resulting in a diminish battery health or even cause thermal runaway (destruction of the battery) [13].

1.2.10. Cycle Life

In literature, it is assumed that the battery has reached its EOL when the capacity is reduced to 80% of the Beginning of Life (BOL) capacity. Cycle life is the number of fully discharge charge cycles until the battery has reached its EOL. Cycle life strongly dependent on C-rate, temperature, and voltage window of the cycles. Higher C-rate, higher voltage window, and operating at extreme temperatures will reduce cycle life [13].

1.2.11. Battery Thermal Management Systems (BTMS)

The Battery Thermal Management System (BTMS) is the device responsible for managing/dissipating the heat generated during the electrochemical processes occurring in cells, allowing the battery to operate safely and efficiently. The inappropriate battery temperature will have a negative impact on the performance, lifetime and safety of the batteries. Therefore, a BTMS is required for every battery system. The primary duty of a BTMS is to keep the batteries in the optimum temperature range and maintain an even temperature distribution in the battery pack.

The thermal management system should be able to maintain a temperature difference of about 2–3 °C from the coolest cell to the warmest cell. At the worst-case condition, usually for larger packs the difference can be as much as 6–8 °C. The reason why this is important is that a large temperature gradient between the cells will cause the cells to age at different rates. So the hotter cells will age faster than the cooler cells, and if there is a large gradient, this could mean that the battery's calendar life will be reduced prematurely.

Afterward, other factors such as weight, size, reliability and the cost must be taken into consideration based on the application of the battery packs.

1.2.12. Heating Design

Battery system designers do not want to heat a battery except for at very low ambient temperatures and even then it should not be a “rapid” heating. Most liquid electrolytes used in modern lithium-ion batteries will begin to experience reduced power at about −10 °C and will begin to freeze at between −20 °C and −30 °C, which makes them unable to provide power at very low temperatures.

In a liquid-cooled system, a heat pump can be added to the overall system to provide warmed liquid through the cooling loop, which will slowly heat up the batteries. Other methods may also be employed such as using a thin-film heater.

In the Telecom Base Station project, the prismatic batteries in the battery pack are not suitable for charging at low ambient temperatures. In order to be charged at the appropriate capacity and speed (C-rate= 0.5C), the surface temperature of the batteries must be at least +5 ℃. At ambient temperatures below +5 ℃, charging rates are very low (C-rate= 0.02C). At these charging speeds, the batteries cannot charge the battery pack in the required time periods. In the absence of power cuts, ambient air conditioning can be provided by air conditioners, while in case of power cut, the heater will need to heat the battery pack to the required temperature in order to charge it in low ambient temperatures.

1.2.12.1. Flexible Foil Heater

The first design is the foil type heater, which is frequently used especially in the refrigerator and automotive sectors, with its defrosting and anti-icing effect. In this heater, there is a heating wire wrapped in 0.1 mm thick Aluminum (Al) foil, which is placed on a 1 mm thick Al plate. While the inner layer of the heater wire has glass fiber wrapped around it, there is 0.7 mm thick silicon material as insulation material on the outer surface.

Figure 1.5. Foil Type Heater Design

1.2.12.2. Film Resistance Heater

Film type heater was used as the second type of heater. In this heater, the heating process was carried out by means of a film-shaped heater element placed on a 1 mm thick Al plate. Double-sided thermal tape is used between the heating element and the Al plate. The bottom layer is the PET layer.

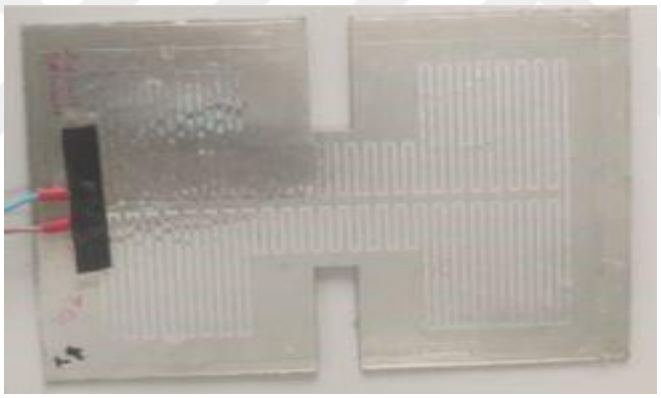

Figure 1.6. Film Type Heater

1.2.13. Cooling System

In liquid-cooled systems with adjustable fluid flow, in the battery high temperatures that may occur can be extracted efficiently. Water-cooled systems have higher thermal capacity than air-cooled systems. Compared to the cooling method with phase change metals, the temperature increase in the battery can be intervened more quickly with water-cooled systems. While the phase change method can only be effective in limited temperature ranges, there are no such restrictions in the water cooling method, provided that it is above the freezing temperature of the water. In the literature, air cooling, phase change materials cooling, liquid cooling systems and their combinations have been tried for BTMS applications.

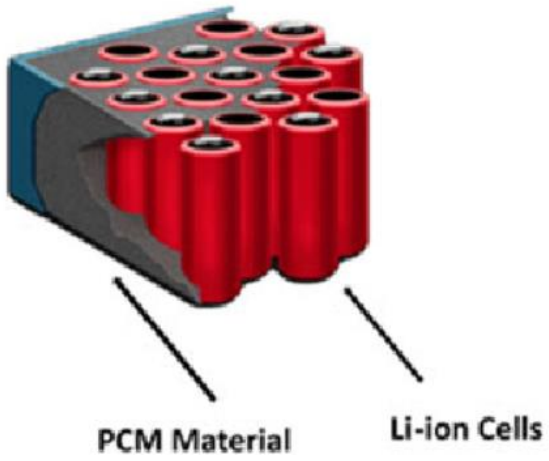

Figure 1.7. Cooling Design with PCM Model [20]

Within the scope of this thesis, the heat generation values obtained from both mathematical calculations and simulations created in the computer environment of the cylindrical and prismatic batteries were verified by performing tests under different conditions in the battery test device. By taking the maximum heat that can occur in the battery as a reference, optimization was made with the channel designs in order to keep the battery temperature at an optimum level below 70°C.

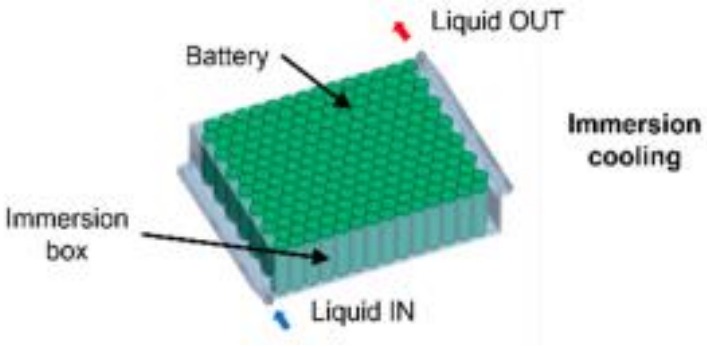

Figure 1.8. Liquid Cooling Design in Battery Systems [21]

In the Energy Storage System (ESS) project, the cooling analysis was performed in two parts. In the first cooling analysis, the discharge of the heat energy that comes out with current flowing through the electronic components (Mosfets, Diodes, Inductors, Resistances) in the Front Panel area where the Battery Management System (BMS) part is located was studied. In this analysis, the design of the cooling area will be discussed after calculating the total amount of heat energy produced. With the Aluminum fin structure to be placed in the cooling area, it will be checked whether it is possible to dissipate the heat naturally. Analyzes will be carried out by making design changes on the aluminum fins to provide the required cooling capacity. As a result of

the analysis, the temperature values of each component on the components will be computed and it will be checked whether they are below the critical temperature values.

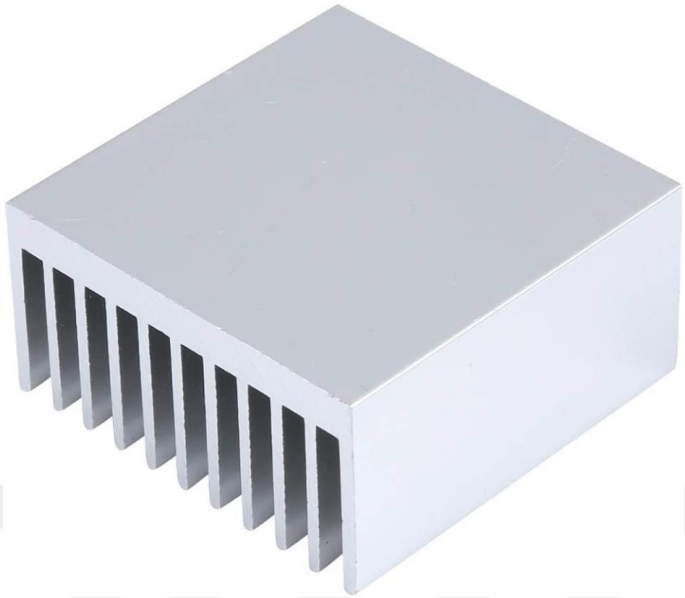

Figure 1.9. Aluminum Fin Structure for Cooling Design [22]

If the temperature values can be kept at the desired values or lower, Aluminum fin structured cooling will be considered sufficient. However, if the temperature values are above the desired values, the appropriate one of the active cooling methods mentioned above will be selected.

In the second cooling design analysis, after the appropriate cooling design decision is made on the front panel, analyzes will be carried out in the entire battery pack including the batteries. In these analyzes, unlike the first front panel cooling analysis, the heat production values of the batteries will be examined under the operating conditions, while the current is passing through them. After these heat generation capacities are determined, they will be included in the cooling analysis. Cooling analysis will be done both on the front panel side and with the batteries. With this analysis, the temperature values on the batteries and the temperature values on the front panel will be checked. If the temperature values in the package are at the desired values or at lower temperature values, the verification studies of the cooling design analyses will be started. However, if the temperatures obtained in the analyzes in the package are above the desired values, studies on the design that is suitable from the active cooling methods will begin.

2. BACKGROUND AND LITERATURE REVIEW

2.1. History of Batteries

A battery is an electrochemical cell that stores electrical energy chemically and converts chemical energy into electrical energy with ionic reactions taking place inside it. It is also a portable storage device containing multiple electrochemical cells that can convert the stored chemical energy into electrical energy with high efficiency and without any gas emission during operation. In the selection of batteries, features such as the dimensions designed for production, the amount of electrical energy they can provide, their portability and whether they are disposable or reusable are taken into account.

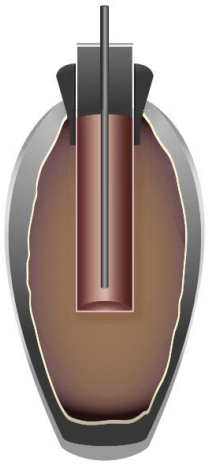

Figure 2.1. Baghdad Battery [23]

The Baghdad Battery is the name given to a set of three artifacts which were found together: a ceramic pot, a tube of copper, and a rod of iron. It was discovered in present-day Khujut Rabu, Iraq, close to the metropolis of Ctesiphon, the capital of the Parthian (150 BC – 223 AD) and Sasanian (224–650 AD) empires, and it is believed to date from either of these periods. When this system is operated today, it is possible to obtain 1.1-2.0 volts of electricity [24].

The first description of the batteries was made in an 1800 study by Volta, who is an Italian professor at the University of Pavia. He invented the voltaic pile in 1800, which is the first form of the battery as we know it today. Since his invention, considerable studies were made and various battery chemistries have been developed [25].

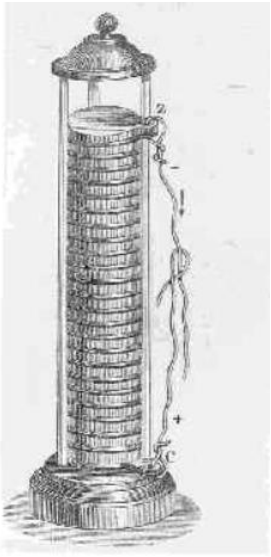

Figure 2.2. Voltaic Pile - the First Electrical Battery, Created c. 1800 by Alessandro Volta [26]

The Daniel Battery (or Daniel Cell, Daniel Cell) is a battery discovered in 1836 [27] by the English chemist and meteorologist John Frederic Daniel. The voltaic battery, in which one metal is oxidized and hydrogen ions are reduced in the other metal, consists of zinc and copper electrodes and is a battery that produces an electrical voltage of about 1.1 volts. Thanks to the electrolyte obtained by mixing sulfuric acid with water or salt water, it became more efficient and became known as the Daniel battery. Each electrode using copper and zinc electrodes is immersed in solutions of its own salts and separated from each other by a porous partition. While the zinc electrode dissolves, copper ions are collected on its own electrode. The chemical reaction that occurs:

$$Zn + Cu^{+2} \rightarrow Zn^{+2} + Cu \tag{2.1}$$

Figure 2.3. Daniel Cells (1836) [28]

In 1860, the Frenchman Gaston Planté (1834–1889) invented the first practical version of a rechargeable battery based on lead–acid chemistry the most successful secondary battery of all ages. Working in Paris as a lecture assistant in physics, Planté began designing a battery that could store a useful amount of electrical energy. The Daniel Cell, the best battery available at that time, was longer-lasting than the voltaic pile, but produced a relatively small voltage (about 1.1V) and was limited by an irreversible chemical reaction. Then, in 1859, Planté succeeded in inventing the first secondary, or rechargeable, battery, named for him. The electrode reactions of lead acid batteries are shown by equations (2.2) and (2.3) [29].

$$\text{Cathode:} \quad \text{Pb}O_2 + H_2SO_4 + 2H^+ + 2e = PbSO_4 + 2H_2O \tag{2.2}$$

$$\text{Anode:} \quad \text{Pb}O_2 + H_2SO_4 + 2H^+ + 2e = PbSO_4 + 2H_2O \tag{2.3}$$

The technology developing day by day with lead acid batteries has advanced with the commercially known Ni-Cd and Ni-metal hydride (Ni-MH) batteries and finally contributed to the emergence of lithium ion battery technology. Primary lithium batteries become commercially available during 1970s. In 1990s rechargeable lithium metal batteries were tried to be developed but faced significant issues in terms of safety and long charging times.

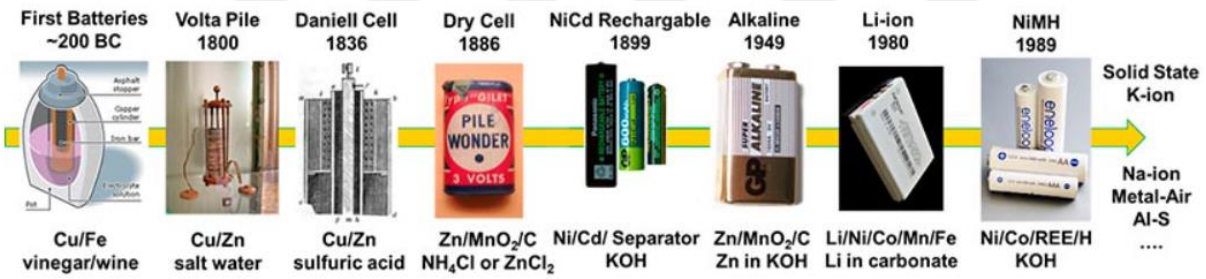

Figure 2.4. History of Batteries [30]

The popularity of lithium batteries was increased and conquered the market by introducing graphite (as opposed to the lithium metal) and lithiated transition metal oxide as anode and cathode materials. As a result, $LiCoO_2$, $Li[NiCoAl]O_2$, $Li[MnNiCi]O_2$ and $LiMn_2O_4$ became the most widely used lithium chemistries in the market.

2.2. Literature Review

The most important problem of batteries consisting of Li-ion cells is balancing the charge state between cells and providing temperature control between the batteries. In order to solve these problems, the mathematical model and simulation of the battery are discussed in detail. In addition, information is given about the general structure and operation of the battery

management system, which provides the control and management of many functions in the battery.

The main purpose of this thesis study is to develop a Battery Thermal Management System (BTMS) model for balancing the different cooling and heating circuits within the battery pack to fulfil the performance requirements. As prerequisites for the modelling, the requirements of the battery pack will be investigated at first through literature research. Then, several potential BTMSs, both in commercial stage and study phase, will be listed in a concept selection matrix with their pros and cons. After the models are built up through simulation tool ANSYS, they will be tested in different initial conditions. Lastly, the corresponding performance parameters of systems will be analyzed and compared.

The operating temperature of the battery should be kept between 20 ºC and 40 ºC to obtain good performance and long lifetime as mentioned above. At very cold temperatures, the battery runs slowly due to high internal resistance. Experimental and numerically different preheating methods were investigated in order to bring the operating conditions to a reasonable temperature range and to obtain a good performance in the prismatic battery module, and a similar preheating study previously was done by Pesaran [31].

It is also important to maintain uniformity of temperatures throughout the battery pack to avoid short-circuiting or local degradation at high temperatures. Considering the temperature dependence of the battery cell voltage, a large temperature change in the battery pack generates unstable battery voltage, leading to a safety issue. For this reason, it is recommended to keep the temperature difference from cell to cell and module to module below 5 ºC [32].

Efficient cooling systems need to be designed to keep the battery within the prescribed temperature range [33]. The battery thermal management system (BTMS) aims to provide effective cooling solutions and also to develop new tools that simulate the behavior of the battery during operation depending on the cooling solution applied. The development of faster model estimation will allow to improve the design process of BTMS and reduce the production cost.

Within the scope of the thesis, studies will be carried out on the equivalent circuit model and the model will be developed by considering the effect of important parameters such as current density, voltage information, state of charge, temperature, aging of the battery from the real lithium-ion battery data required for this model. In the verification of the developed mathematical model, the battery characteristics shared by the manufacturer will be compared with the results of the current density tests performed on the battery sample and the model outputs will be compared to the measurements. ANSYS Fluent software will be used to solve

the temperature distributions and the check the accuracy of the thermal management system model.

As a result of the modeling and simulation studies, a control and management strategy has been put forward that will improve the overall performance of the battery pack by eliminating the imbalance in temperature distribution between the battery cells.

3. METHODOLOGY

3.1. Mathematical Model

3.1.1. Multi Scale Multi Dimension (MSMD) Battery Model

The MSMD approach deals with different physics in different solution domains [21].

Computational Fluid Dynamics (CFD) is used to solve thermal battery and electrical field using the following differential equations [22]:

$$\frac{\partial_\rho C_p T}{\partial t} - \nabla.(k\nabla T) = \dot{q} \tag{3.1}$$

$$\nabla.(\sigma_+ \nabla\varphi_+) = -j \tag{3.2}$$

$$\nabla.(\sigma_- \nabla\varphi_-) = j$$

where σ_+ and σ_- are the effective electric conductivities for the positive and negative electrodes, φ_+ and φ_- are phase potentials for the positive and negative electrodes, j is the volumetric transfer current density computed from an electro chemical sub-model, and $\dot{q}$ is the heat generation rate during a battery operation, which includes Joule heating, electrochemical reaction heating, and entropic heating.

In MSMD Battery Model, the following electrochemical sub-models are implemented; Equivalent Circuit Model (ECM), The Newman, Tiedemann, Gu, and Kim (NTGK) Model and Newman P2D Model.

Equivalent Circuit Model (ECM)

An electrical circuit representation is used to simulate battery electric behavior. ANSYS Fluent has been used with six parameters in ECM [23]. In this model, the circuit includes three resistors and two capacitors.

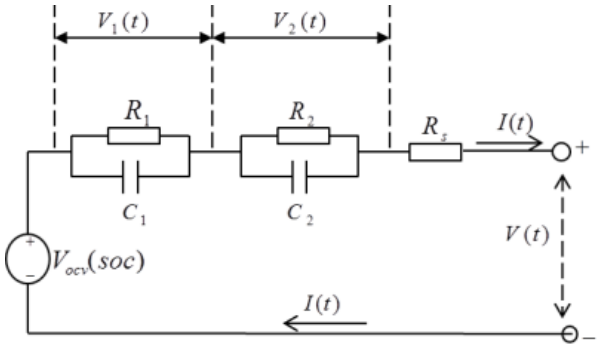

Figure 3.1. ECM Model representation [37]

The open circuit voltage, resistances, and capacitances depend on the battery SOC. In ANSYS Fluent, these functions are represented in polynomial form as:

$$R_s = a_0 + a_1(soc) + a_2(soc)^2 + a_3(soc)^3 + a_4(soc)^4 + a_5(soc)^5 \quad (3.3)$$

$$R_1 = b_0 + b_1(soc) + b_2(soc)^2 + b_3(soc)^3 + b_4(soc)^4 + b_5(soc)^5 \quad (3.4)$$

$$C_1 = c_0 + c_1(soc) + c_2(soc)^2 + c_3(soc)^3 + c_4(soc)^4 + c_5(soc)^5 \quad (3.5)$$

$$R_2 = d_0 + d_1(soc) + d_2(soc)^2 + d_3(soc)^3 + d_4(soc)^4 + d_5(soc)^5 \quad (3.6)$$

$$C_2 = e_0 + e_1(soc) + e_2(soc)^2 + e_3(soc)^3 + e_4(soc)^4 + e_5(soc)^5 \quad (3.7)$$

$$V_{OCV} = f_0 + f_1(soc) + f_2(soc)^2 + f_3(soc)^3 + f_4(soc)^4 + f_5(soc)^5 \quad (3.8)$$

In the equation set, the open circuit voltage V_{ocv}, resistors' resistances R_s, R_1 and R_2 and capacitors' capacitances C_1 and C_2 are functions of the battery's state of charge SoC and possible temperature.

Newman, Tiedemann, Gu, and Kim (NTGK) Model

NTGK Model [38] is a semi-empirical electrochemical method. It was improved by Kwon [39]. In the model formulation, the current transfer is related to the potential field by the following algebraic equation:

$$j = \alpha Y[U - (\varphi_+ - \varphi_-)] \quad (3.9)$$

where α is the specific area of the electrode sandwich sheet in the battery, Y and U are the model parameters which are functions of the battery DoD:

$$DoD = Vol/3600.\, Q_{Ah} \left(\int_0^t j dt\right) \quad (3.10)$$

where Vol denotes the battery volume, and Q_{Ah} is the battery total electric capacity in Ampere hours.

Newman P2D

Newman's group developed a physics based model using porous electrode and concentrated solution theories [40]. The model can accurately capture Li-ion migration in the battery. It has been widely used in the literature.

Figure 3.2. shows the electrode plate pair in the Li-ion battery. Li diffuses to the surface of negative electrode particles during the discharge process. Then it undergoes an electrochemical reaction. This reaction releases an electron and transfers Li to the electrolyte phase. The Li+ ions diffuse through the electrolyte to the positive electrode, where a similar reaction transfers Li+ to the positive solid phase. Li is stored inside the positive electrode particles until the cell

is later recharged. The Li-ion transport phenomena in the porous electrode and active particle material can be described by the charge and mass conservation laws [37].

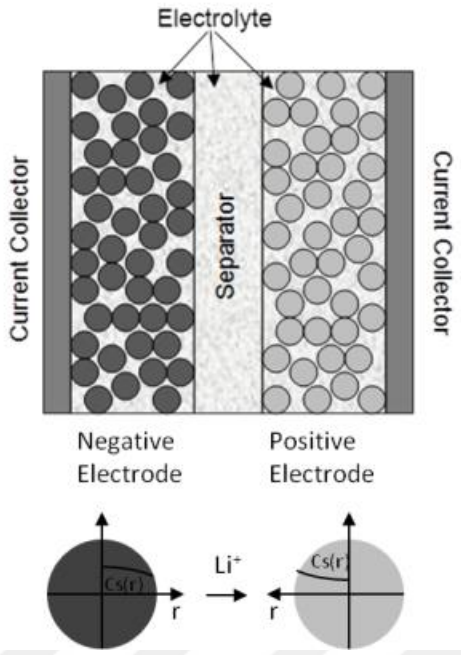

Figure 3.2. Newman Model [37]

3.2. Test System and Procedure

To extract all the parameters in the proposed model, a battery test system and an experimental procedure were designed to measure batteries conveniently and efficiently. The basis for the testing is to analyze and map the rise of temperatures and the progression of heat transfer during discharge. The data from these tests are used to calibrate the simulations by comparing the simulation result versus the real-life testing results. The result from the simulation can also be used for later comparison with all the conceptual designs through design studies. The tests and simulations are used to help understand the transfer of heat and later can be used as a baseline for concept development of the new battery packs.

3.2.1. Test Equipment

Thermal performance tests are performed for both single and packaged batteries with the Giant Force devices shown in Figure 3.3. Appropriate tests are carried out by bringing the cabin to the desired climatic conditions for the test conditions. It allows appropriate tests to be performed for the electrical characteristics of individual batteries and battery packs required for electrochemical analysis. The electrical operating range for a single battery is the highest current of 1200A, voltage range -5~5V.

Figure 3.3. Giant Force Test Equipment

As for the electrical operating range for the battery pack, the highest current is 1200A, the voltage range is -10V ~ 100V. In general, the tests applied to single batteries and battery packs with this tester are as follows; capacity and energy characteristics, charge and discharge in different current, power and resistance, retention of charge and charge recovery, storage capability, cycle life and calendar life.

Chroma's models 17020 and 17011, shown in Figure 3.4, are high precision systems specifically designed for secondary battery modules and package testing. Highly accurate sources and measurements ensure that the test quality is suitable to perform repetitive and reliable tests. This is crucial for battery modules / packs, for both incoming and outgoing inspections as well as capacity, performance, production and qualication testing. The channels can easily be paralleled to support higher current requirements. This feature provides the ultimate flexibility between high channel count and high current testing.

Figure 3.4. Chroma 17020 and 17011 Test Equipment

Experiments that can be done with Chroma test devices are capacity test, life cycle test, performance test, reliability test, over charge/discharge test and thermal test. In order to predict the temperature behaviour during various discharge rates, extreme environmental conditions and for cycling procedures of a battery cell alone or in a module, different models have been proposed.

Figure 3.5. Flir E30 Thermal Camera Test Equipment

Flir E30 model thermal camera device seen in Figure 3.5. is used to monitor the temperature distributions on the battery packs locally. The hottest and coldest surfaces can be seen on the device. Temperature range is from -20°C to 120°C with an accuracy of 2%.

In addition to thermal cameras, sensitive type thermocouples and NTC sensors integrated with PCB board are used for temperature measurements. According to the working conditions in the experiments and the sensitivity of the experiments, the appropriate measurement method and suitable temperature measuring device are preferred. In some sensitive cases, temperature measurements are made with several different methods and the results are compared with each other.

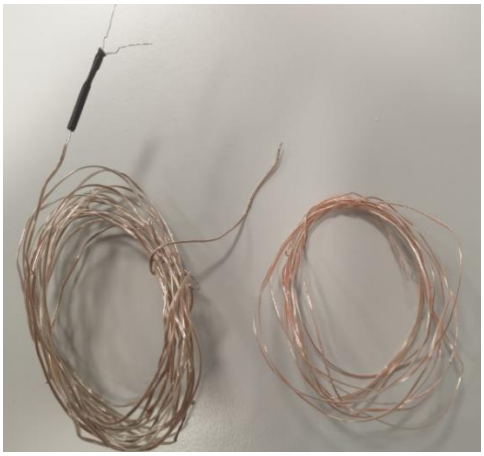

Figure 3.6. K type Thermocouples used in Projects

With K type thermocouple temperature measuring devices, temperature measurements are conducted on the products or on the parts. These thermocouple sensors are regularly calibrated every year. The temperature values measured by the thermocouple devices are read and recorded using a data logging devices (Data Logger), for the BMS card on the battery pack or the Chroma devices in the laboratories. Time intervals in the records taken depending on time are adjusted in the desired ranges. At least one thermocouple is placed in the battery pack for each battery with a critical temperature.

4. RESULTS

Two battery modules with different types of batteries and different usage areas were studied within the frame of the study. Both the vacuum cleaner battery module with a lower capacity and simpler battery system and the ESS battery pack which is a more complex battery module with a higher capacity were studied. In addition, the performance of cooling and heating systems were also examined. First, a single cell battery model of LG 18650 type was developed in commercial software ANSYS Fluent version 2021.R1. to simulate the electrochemical reactions under normal discharge operation and obtain the corresponding heat generation characteristics from a single cell. Performance test results for a single battery were introduced as HPPC data as input in the simulations done with ANSYS Fluent Battery Module. In the battery package analysis, the batteries that heat up the most and the ones that heat the least were determined. Afterwards, temperature measurements were held by NTC temperature sensors and thermocouples located on these batteries in the experiments. The results of the analyzes and experiments were compared and the level of consistency with each other was evaluated. In addition, this analysis was used to enter the Battery parameters into the ANSYS Fluent program and verify the results. This methodology is repeated for subsequent more comprehensive analyses.

4.1. Experimental Results

HPPC data experiments were first performed with the cylindrical batteries used in the Vacuum Cleaner project. In these experiments, the single battery was tested at different ambient temperatures and different SOC levels. The time-dependent changes of SOC and voltage values were measured at different temperatures. These experiments were performed at certain C-rate values. The purpose of the first experiment is to obtain the necessary input values for the analysis of the batteries in the Vacuum cleaner battery.

The second experimental study for this project is thermal analysis experiments that deal with the whole battery pack. In this experiment, it is aimed to examine the thermal performance of the battery pack, the temperature distributions inside the battery. With this distribution, the most critical and sensitive points in the package were obtained. It will be ensured that the temperatures are kept below the predetermined levels with the sensors to be placed at these most critical points during the use of the battery pack together with the device.

In the Telecom base station battery pack, which is designed and developed for base stations as energy storage systems, is different from the vacuum cleaner battery. The need for heating design and cooling design arose due to the working places and ambient conditions. Also, unlike

the cylindrical batteries in vacuum cleaner battery pack, prismatic batteries are used in this battery pack. In order to see the thermal performance characteristics as a standard, HPPC experiments and thermal performance tests were carried out on this Telecom base station package.

4.1.1. Vacuum Cleaner HPPC Experiments

This experiment aims to identify the parameters required to simulate the dynamic electrochemical behavior of the battery cell which will then be used to estimate the heat generation within the cell caused by reversible and irreversible effects under different initial conditions.

By relying on accurate performance models, Li-ion batteries can be tested by simulations considering different scenarios, thereby reducing the laboratory testing efforts that are usually cost demanding and time consuming. In order to build these models, the behavioral characteristics of the battery should be derived by experimental methods. [41]

Table 4.1. LG INR 18650 Product Specification [42]

Item	Condition / Note	Specification
Energy /Capacity	By Std. charge/discharge	Nom. 12.5Wh (3440 mAh) Min. 12.1Wh (3330 mAh)
Nominal Voltage	Average by Std. charge/discharge	3.63 V
Standard charge	Constant current (1C=3333 mA) Constant voltage End condition(Cut off)	0.3C (1000 mA) 4.20 V 50 mA
Standard Discharge	Constant current End condition(Cut off)	0.2C (670 mA) 2.50 V
Min . Discharge Voltage	In all measurements and operations of the cell, the minimum allowable closed circuit voltage shall not be below the following value	2.50 V
Operating Temperature (Atmosphere Temperature)	Charge Discharge	0 ~ 45 ℃ -20 ~ 55 ℃
	*Max. cell surface temperature should be below 75 for discharging	

LG INR18650 type batteries are used in the vacuum cleaner battery pack. The experiments were carried out based on the values specified in the technical data sheet of the cell manufacturer. Technical details of the battery are given in Table 4.1. The critical values at the time of charging and discharging and the values to be taken as a basis in terms of temperature are given in the table.

Before the thermal performance of the battery pack, HPPC experiments were carried out for the electrical characteristics of individual cells. In these experiments, voltage values were measured depending on the SOC levels of individual batteries. Figure 4.1. below shows the typical discharge-voltage graph of a single Li-ion battery.

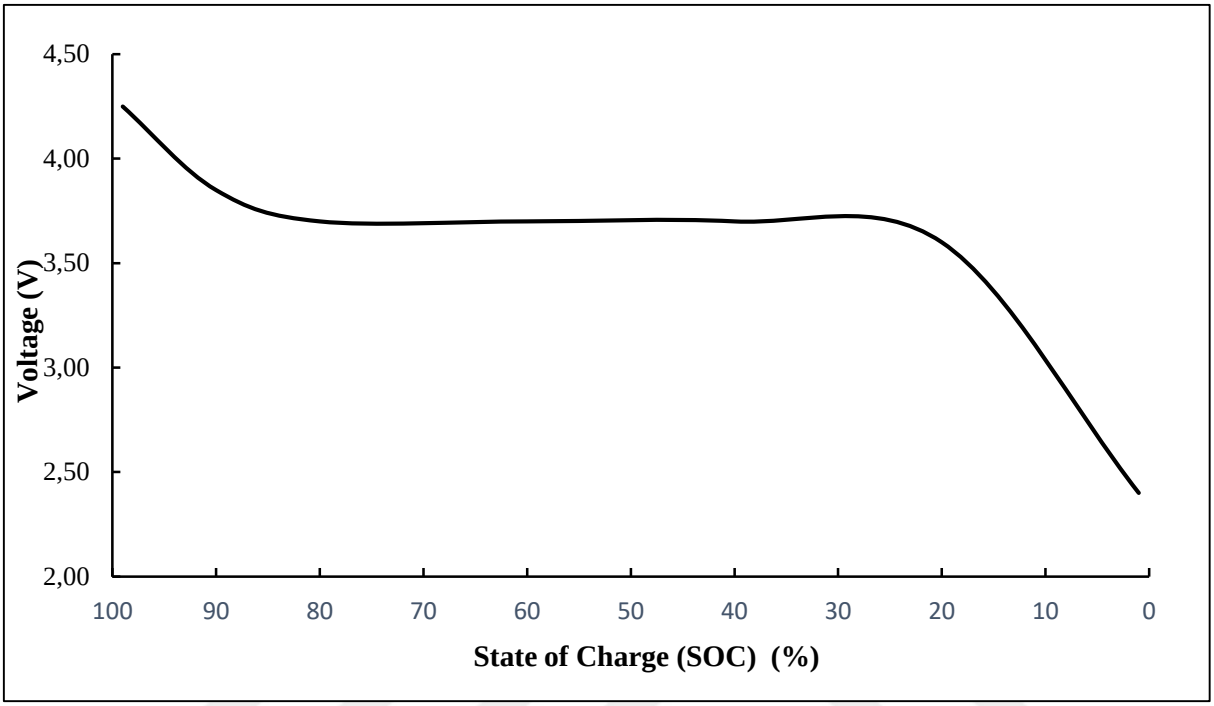

Figure 4.1. LG INR 18650 Li-ion Battery Discharge Voltage Curve

In the HPPC experiment, when the battery was fully charged (SOC=100%), the experiment was started and then voltage levels were measured depending on the change in the SOC level over time. This experiment was repeated for each battery and the test data were recorded separately. These values, afterwards, were entered to the program as a text file as a parameter in the ANSYS Fluent Battery Module analysis.

4.1.2. Vacuum Cleaner Battery Thermal Discharge Experiments

Experiments were carried out in a laboratory to see the temperature distributions inside the vacuum cleaner battery pack. Temperatures were recorded with temperature sensors placed at the maximum temperature points seen in ANSYS Fluent thermal analysis. In addition, thermocouples are located on each battery in order to make detailed comparisons with the analysis. The location of temperature sensors on the vacuum cleaner battery pack is shown in Figure 4.2.

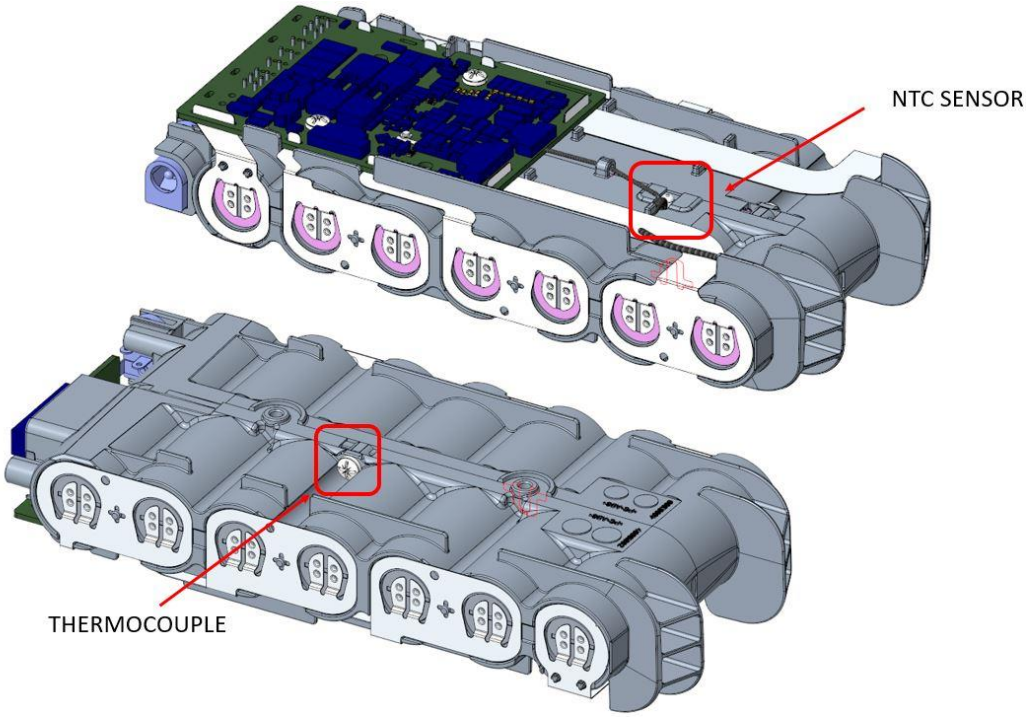

Figure 4.2. Location of Temperature Sensors on Vacuum Cleaner Battery Pack

Battery Pack thermal experiments were performed in Giant Force conditioning cabinets in the Laboratory. The ambient temperature in the cabin was kept at 23.5℃ during the whole experiment. Figure 4.3. shows the placement of the battery pack in the conditioning cabinet.

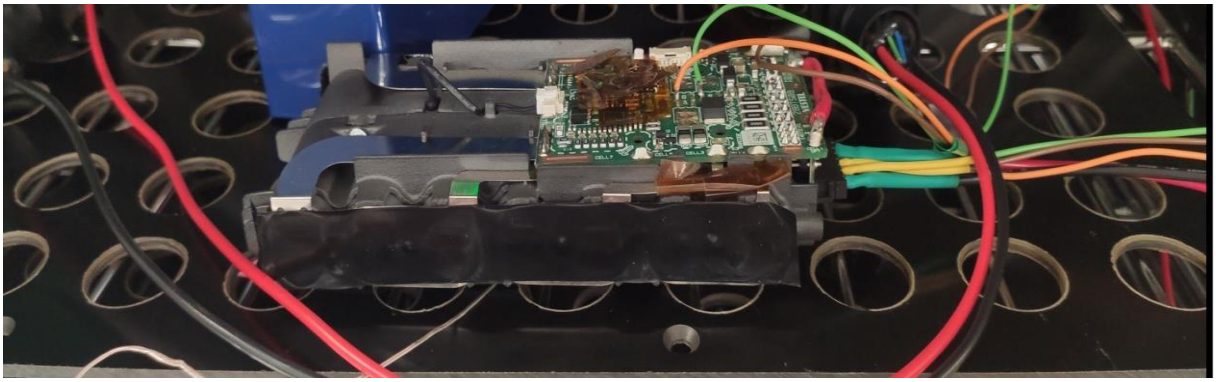

Figure 4.3. Placement of vacuum cleaner battery pack inside the air conditioner

Temperature values were obtained from thermocouple sensors placed on seven batteries in the battery pack. The experiment was started in the fully charged state of the battery (SOC=100%).

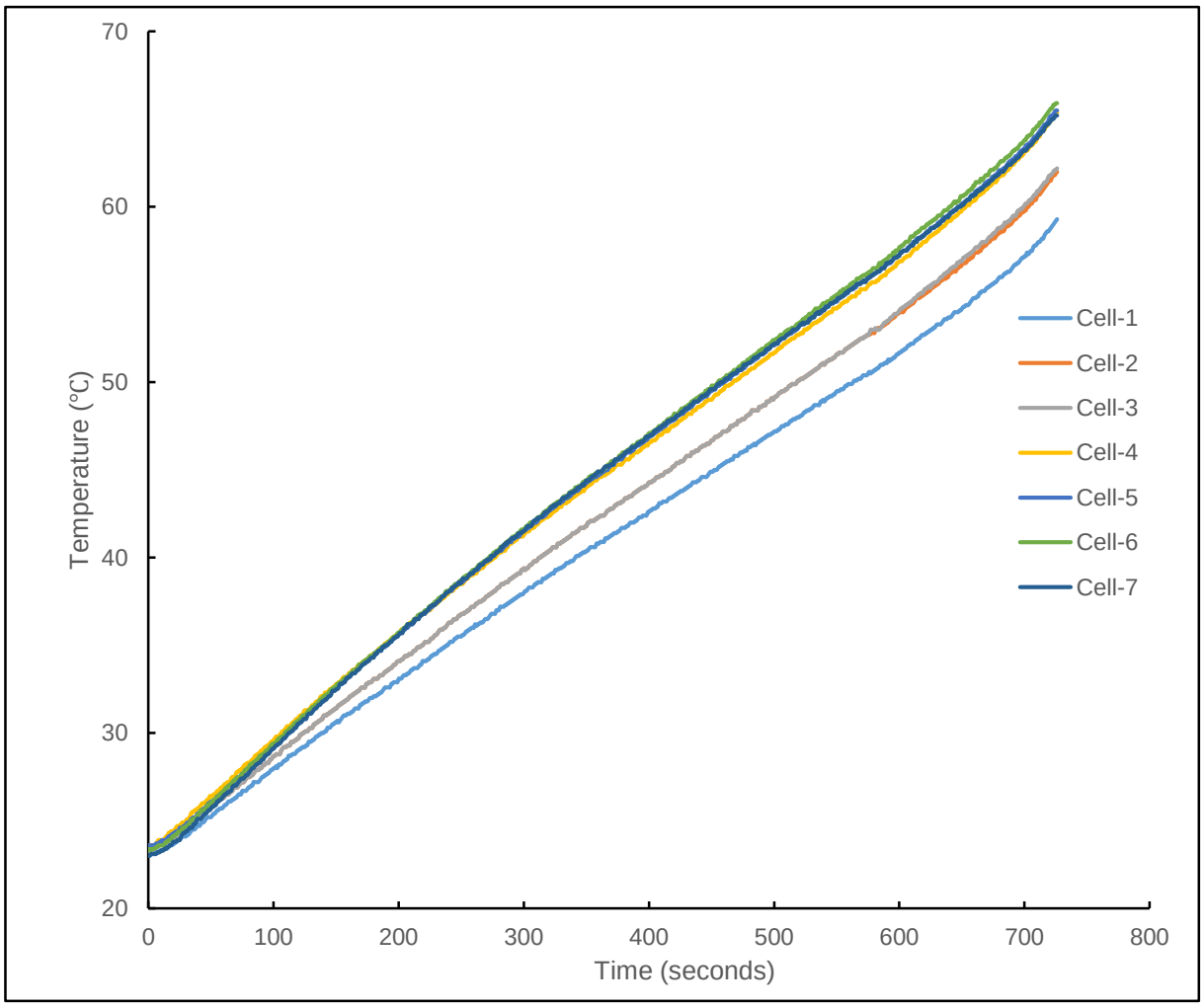

Figure 4.4. Thermal Experiment Results of Seven Cells in Vacuum Cleaner Battery Pack

Surface temperatures were read on each battery over time. Time-dependent temperature measurement results are shared in Figure 4.4.

The experiment was performed at a discharge current of 12 Amps, at a discharge rate of 1C (C-rate=1). Batteries were tested at full capacity. The experiment was continued until the SOC level was 0% and the capacity was completely exhausted. It took 730 seconds for the batteries to be completely discharged. During this period, temperatures were measured from each battery with thermocouples and these values were recorded using the Data Logger device.

4.1.3. Heater Thermal Experiments for Telecom Base Station Battery

In the Telecom Base Station project, the prismatic cells in the battery pack are not suitable for charging at low ambient temperatures. In order to be charged at the appropriate capacity and

speed (C-rate= 0.5C), the surface temperature of the cells must be at least +5 ℃. The cells can be charged at very low C-rates with surface temperatures of -5 ℃ to +5 ℃. However, it will take a very long time to charge in this temperature range and low temperatures on the cells will adversely affect. At temperatures below -5 ℃, the cell manufacturer states that the cells should never be charged. At ambient temperatures below +5 ℃, charging rates are very low (C-rate= 0.02C). In the absence of power cuts, ambient air conditioning can be provided by air conditioners, while in case of power cut, the heater will need to heat the battery pack to the required temperature in order to charge it in low ambient temperatures.

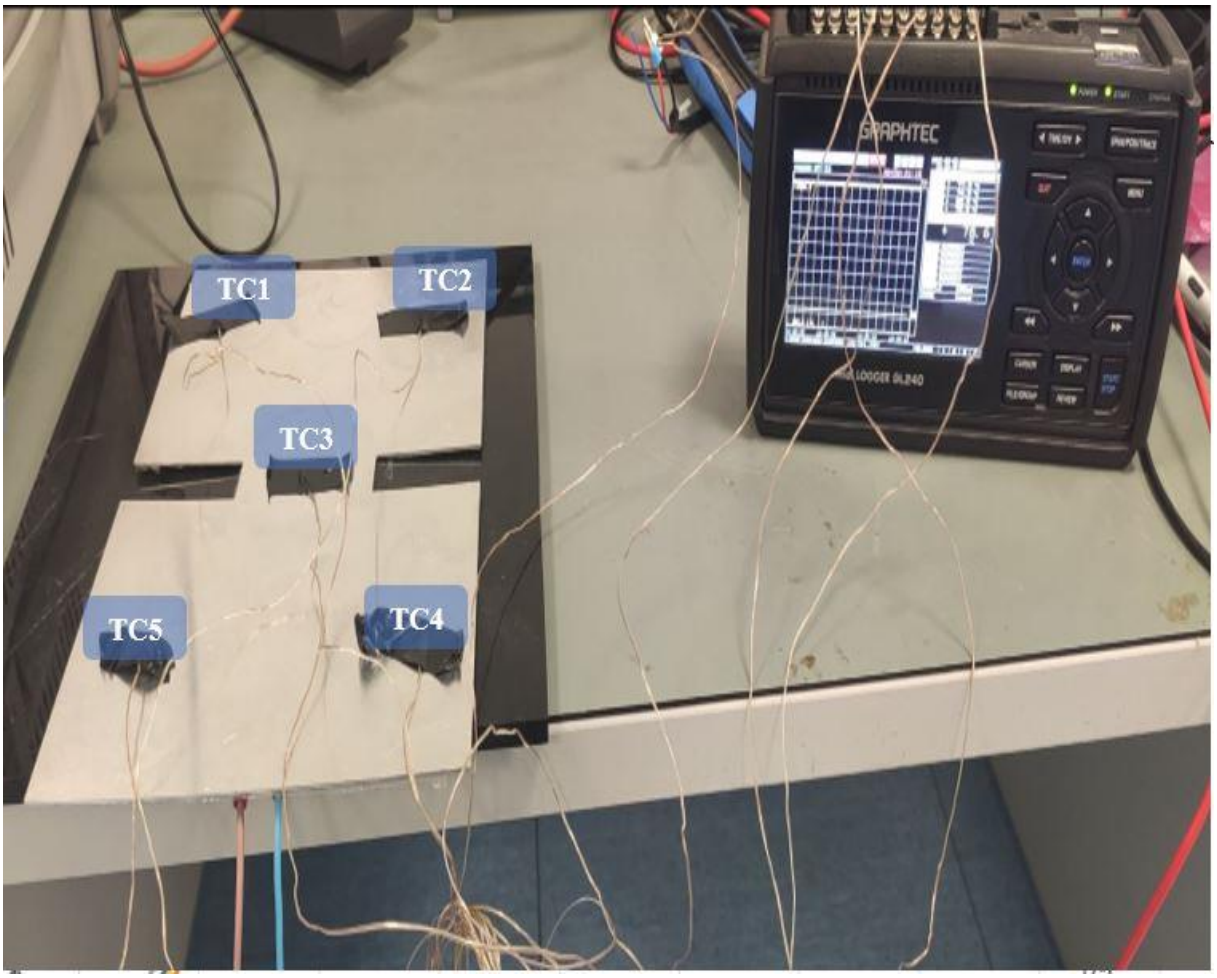

Figure 4.5. Heater experimental setup

In Figure 4.5, TC denotes 'Thermocouples' affixed to the heater. 5 thermocouples are attached to the heater. The tests were started in the test stand at an ambient temperature of 25℃. Thermocouples are located to 5 different points on each heater. Values from Thermocouple measurement sensors were recorded in the Data Logger device. With the data logger device, 10 measurement data were taken in 1 second.

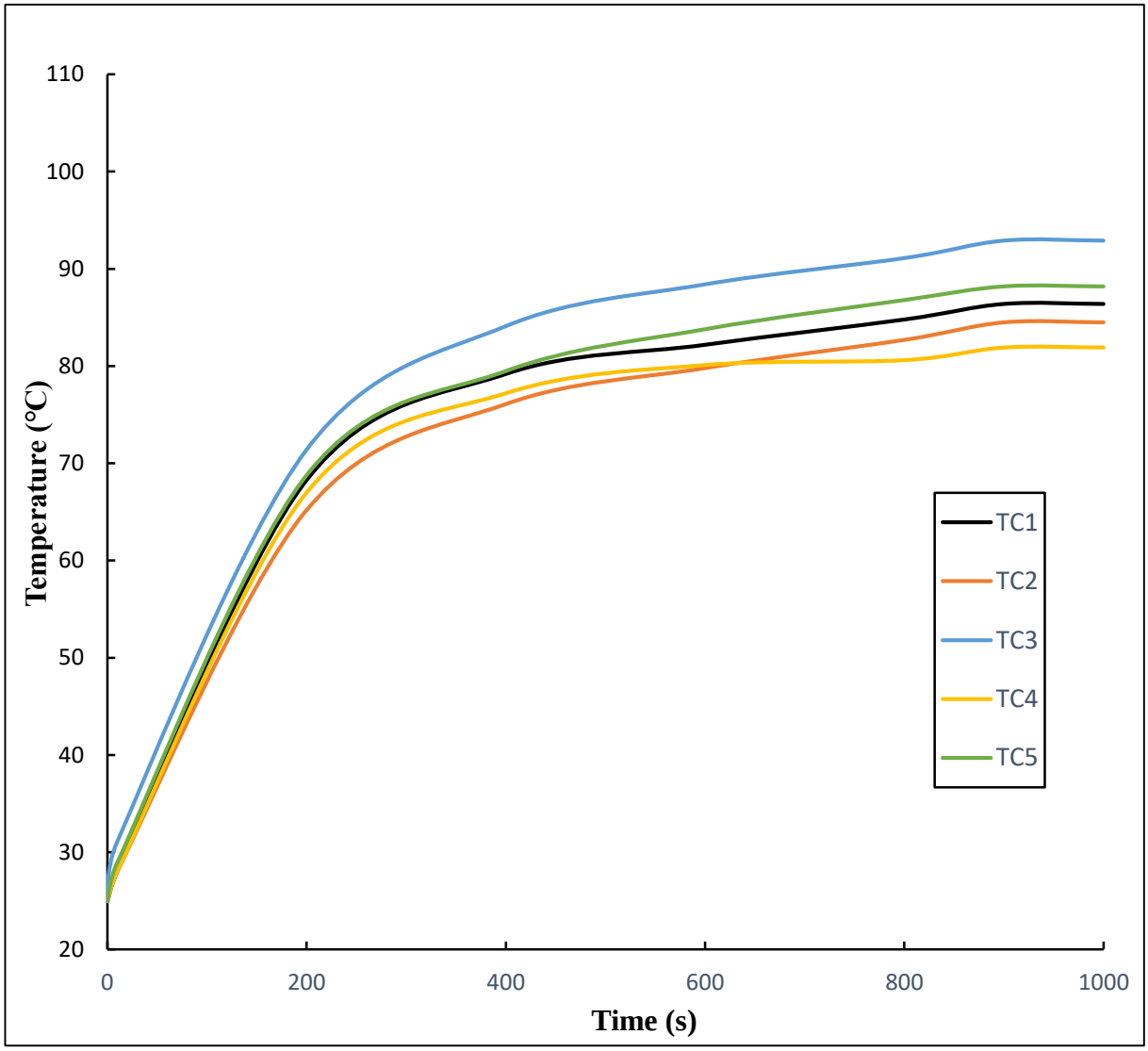

Figure 4.6. Film Type Heater Thermal Experiment Results for Five Points

Figure 4.6 shows the temperature results of the film type heater under the specified test setup and conditions.

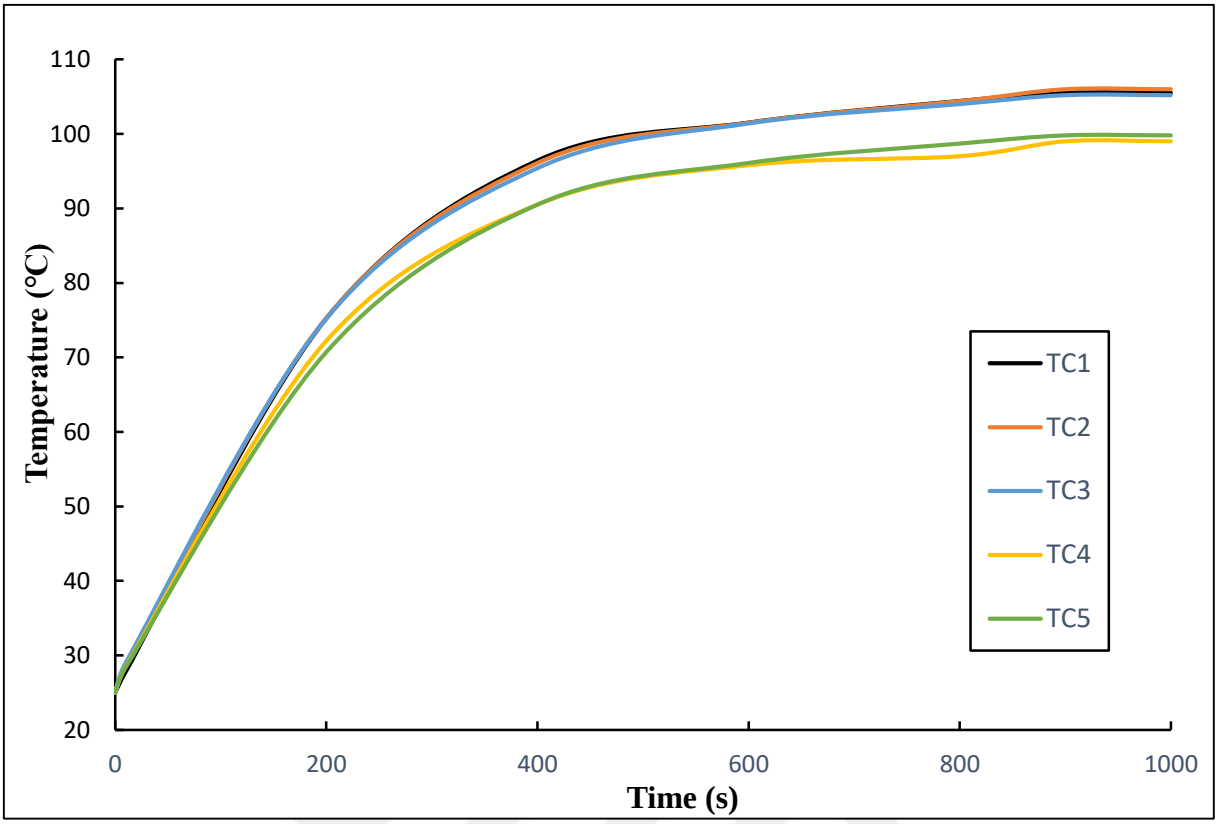

Figure 4.7. Foil Type Heater Thermal Experiment Results for Five Points

The tests were started in the test stand at an ambient temperature of 25 ℃. Thermocouple is connected to 5 different points on each heater.

4.1.4. Telecom Base Station Battery HPPC Experiments

Prismatic type cells were used in the Telecom Base Station project designed for ESS. HPPC testing was performed to determine battery performance. HPPC tests were carried out in cabinets where the ambient temperature was kept under control. The test start temperature is 25 ℃ at room temperature. While the batteries are being discharged, the cut-off voltage and the charging method are based on the method determined by the manufacturer. The steps and sequence applied while performing the capacity test are shown in the Table 4.2 below.

Table 4.2. Capacity Test Steps at Room Temperature

Step	Procedure	Cabinet Temperature	Time (Hour)
1	Thermal Balance	25 ℃	4
2	Discharge (1C) (Cut-off = 2,5 V)	25 ℃	1
3	Standby Time	25 ℃	1
		Total Time	6

At 25 ℃ room conditions, the batteries were kept in the cabinet for 4 hours to ensure thermal equilibrium conditions. The batteries were fully charged before the HPPC test started. The

voltage values of the fully charged batteries are 3.3 V. The capacity value in the fully loaded position is 100 Ah. This value represents 100% on the SOC chart. After the discharge process starts, the capacity value starts to decrease with the decrease of the voltage value. The voltage value drops from 3.3 V to 2.5 V. When the battery is fully discharged, the voltage becomes 2.5 V and the capacity value drops to 0 Ah. On the SOC graph, 0 Ah represents the 0% position.

Table 4.3. CALB L160F100A Product Specification [43]

Item	Condition / Note	Specification
Energy /Capacity	Standart discharge	Nom. 100 Ah Min. 100 Ah
Working Voltage	at room temperature	2.50 V - 3.65 V
Standard Charging Model	at room temperature	Charged to 3.65V at a constant current of 50A, and then, charged continuously with constant voltage of 3.65V until the current was not more than 5±0.5A.
Standard Discharging Model	at room temperature	Discharge to 2.5V at a constant current of 100A.
Absolute Charging Temperature	No matter what the charging model is, once the temperature of the cell is above the absolute charging temperature, charging should be stopped.	-5 ℃ ~ 55 ℃
Absolute Discharging Temperature	No matter what the discharging model is, once the temperature of the cell is above the absolute discharging temperature, discharging should be stopped.	-20 ℃ ~ 60 ℃

The information shared by the prismatic battery manufacturer company for the healthy and safe operation of the batteries is shared in detail in Table 4.3. The charge and discharge processes were tested in HPPC tests by considering this information.

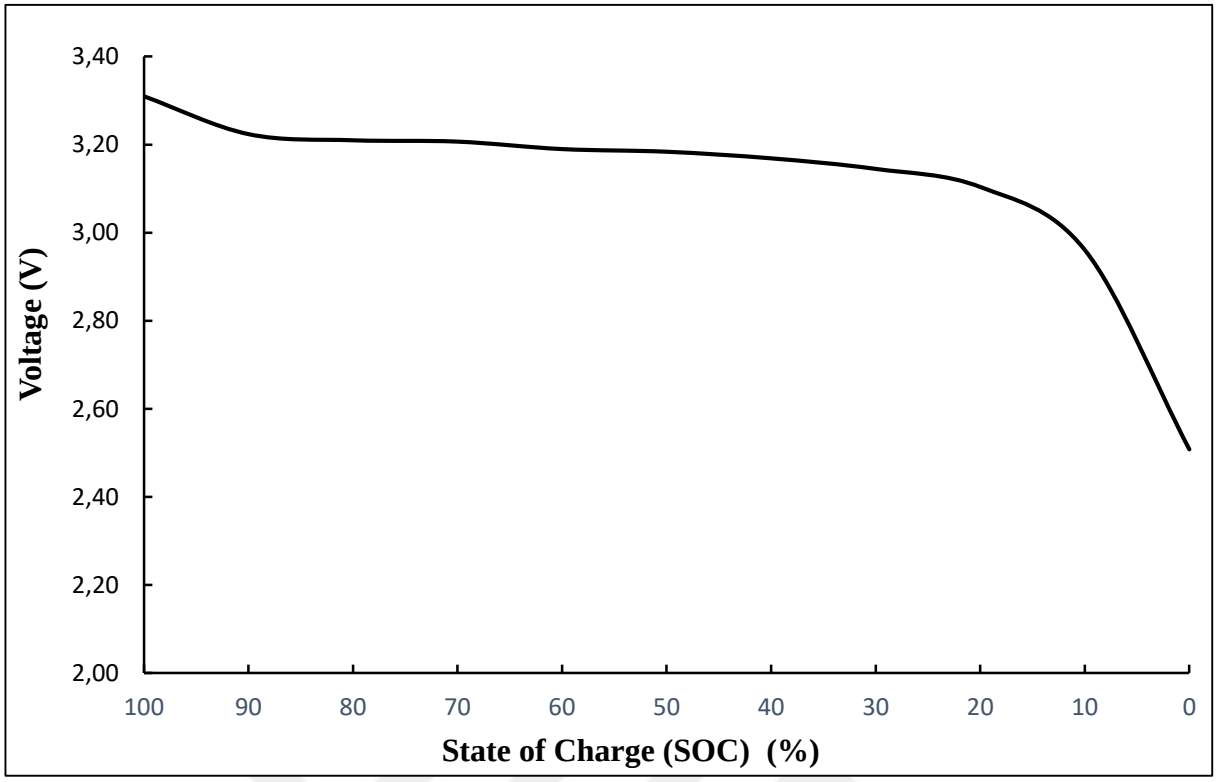

Figure 4.8. L160F100 Prismatic Li-ion Cell Discharge Voltage Curve

In Figure 4.8, the Voltage-SOC graph shows the variation of Voltage and SOC over time. The discharge process was carried out at C-rate of 1C and 50 Amperes. The discharge experiment took approximately 1 hour. During this period, the batteries reached a cut-off value of 2.5 V from the fully charged position. After the discharge process was completed, the experiment was not terminated immediately and the experiment was terminated after waiting for 1 hour in the cabinet at ambient temperature in order for the batteries to reach thermal equilibrium.

4.1.5. Telecom Base Station (TBS) Battery Thermal Discharge Experiments

In order to determine the temperature distributions and differences of the cells during charge/discharge in the TBS Package, the experiment was performed by connecting external Thermocouples. A total of 15 thermocouples were connected in the experiment. The applied test procedure and cycle are as shown in the Table 4.4 below.

Table 4.4. Test Procedure of Thermal Discharge Experiment

Step	Procedure	Cabinet Temperature	Time (Min)
1	Thermal Balance	20 ℃	300
2	Charge (0.5 C)	20 ℃	150
3	Standby Time	20 ℃	30
4	Discharge (0.5 C)	20 ℃	120
5	Standby Time	20 ℃	30

The test was terminated by repeating the charging and discharging processes given in the Table 4.4 (processes between 2-5 numbers) 3 times. Thus, the test period took a total of 21.5 hours. After recording the three measurement results, the consistency of the tests with each other was checked. At the beginning of the three tests, it was waited for the cells to reach thermal equilibrium. Approximately 30 minutes waited between tests to reach thermal equilibrium. After the cells reached thermal equilibrium, the next cycle was restarted.

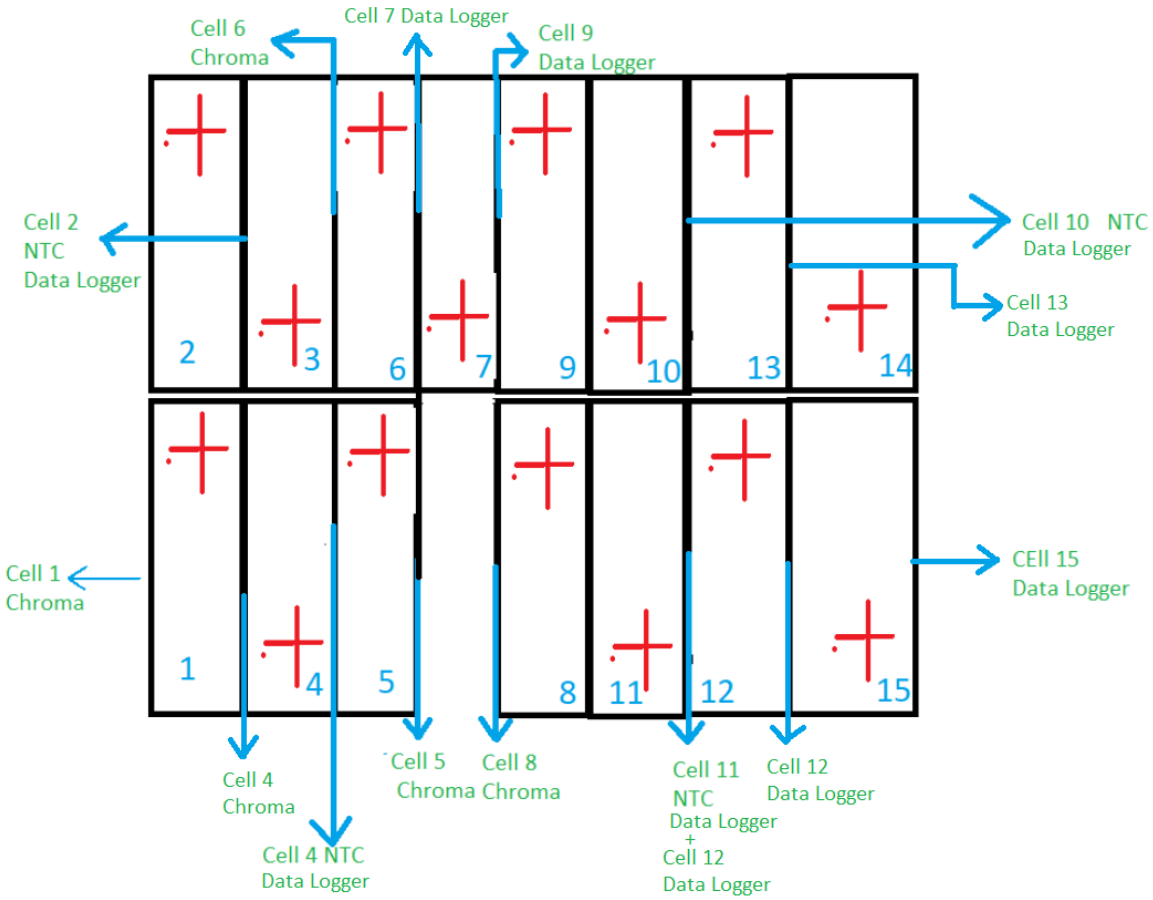

Figure 4.9. Location of Thermocouples and NTC Sensors on the Battery Pack

Thermocouples are mounted on the side surfaces of the cells by means of thermal tapes. Surfaces that were identified as critical in ANSYS Fluent analysis were determined and the temperatures were measured by sticking them to these surfaces. Both NTC sensors and thermocouples are placed on the surfaces to ensure that the values are measured correctly on critical surfaces. The values measured on both sensors were compared with each other and the measurement consistency was checked.

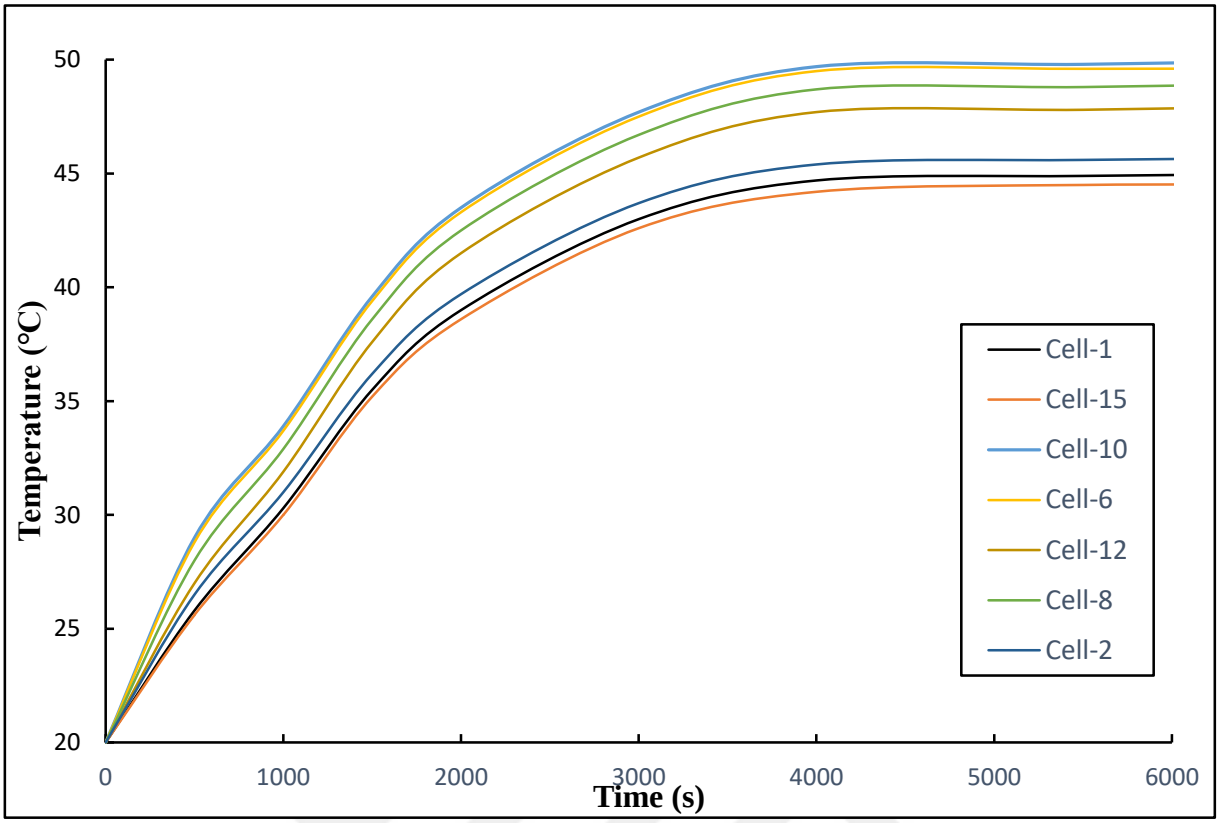

Figure 4.10. Cell Temperatures Taken from Data Logger and BMS During Discharge

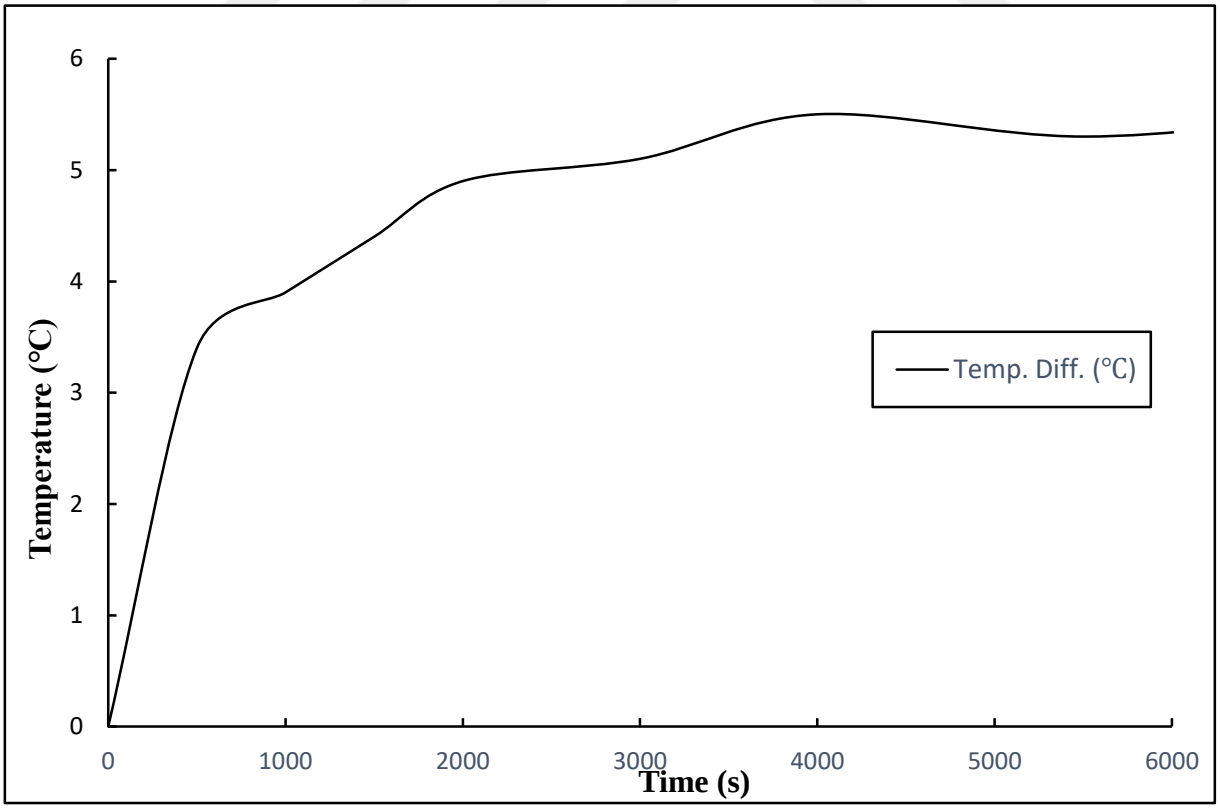

Figure 4.11. Time-Dependent Variation of the Maximum Temperature Difference Between Cell10 and Cell 15

As seen in Figure 4.11, Thanks to the thermocouple sensors placed on the critical cells on the battery pack, the temperatures were recorded during the discharge. While the warmest cells are seen as cell 10, cell 6 in the middle, the coldest cells are seen as cell 1, cell 15 and cell 2. The maximum temperature difference between the Cells during discharge was found to be 5.5 °C at the end of the test, as seen in Figure 4.12.

4.2. Numerical Results

In order to give direction to the design studies, first of all, numerical analysis studies were carried out for each project. With the design studies, it is envisaged to save on extra model and experiment costs. In addition, the extra time to be spent on experiments and prototype studies is prevented.

Since the cylindrical batteries used in the vacuum cleaner project are currently used in standards, the issue of thermal management has been more comfortable. Analysis studies required for both electrochemical analysis processes and thermal management and design were resolved more quickly. As a result of the analysis studies, the appropriate design and sensor placement were determined. It has been determined in the analysis that which batteries how much will heat up and which batteries will have higher temperature increase. As a result of the analysis, NTC sensors were placed between the hottest batteries. These NTC sensors transfer the temperature values to be read on the batteries during charging and discharging to the BMS. In this way, temperature control will be provided on the battery pack.

The thermal analysis studies in the TBS battery pack is more important than in the vacuum cleaner project. One of the biggest reasons for this is that the use of prismatic batteries is not very common. Therefore, it is very important to extract the thermal characteristics of the batteries. In addition, considering the number of batteries used and all costs of the battery pack, minimizing the number of prototype studies and experimental studies will provide a great cost savings.

Analysis of the preheating system and the cooling system of the battery pack, which will be designed separately in the TBS project, is more complicated. Further analysis of the BTMS structure was required in this project. In particular, different analysis studies and parameters were used to decide on the method to be chosen in the design of the cooling system.

4.2.1. Model Development and Verification Study Using a Cylindrical Li-ion Vacuum Cleaner Battery

The Lithium-ion battery pack is composed of 7 cells connected in series. Based on the thermal model developed for LG INR18650M36 single cell, the thermal behavior of the battery pack can be simulated. The model of a typical 25.2 V 3.4Ah 18650 battery pack is shown in Figure 4.12 Seven identical cells are packed in the form of 1x7 closely. The adjacent pairs of the batteries are linked with Nickel coated Copper tabs to achieve serial connection of the batteries.

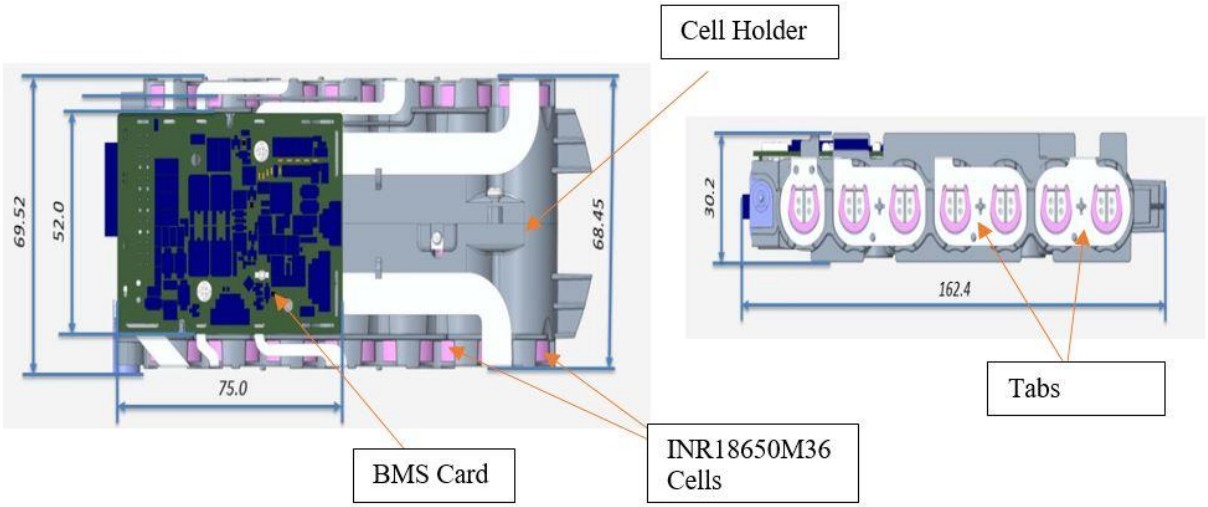

Figure 4.12. Geometry of the Vacuum Cleaner Battery, a) Front view of Batteries with BMS Card, b) Top View of Batteries and Tabs

In Figure 4.12.a and 4.12.b, there are front view, top view and general dimensions of the vacuum cleaner battery, respectively. Temperature changes in the discharge state of the battery pack were analyzed. Time-dependent results were found for each battery's 12 ampere discharge current, and then the batteries that reached the highest temperatures were determined. NTC sensors were placed on these determined batteries. Temperature information from sensors is controlled by BMS. The control of the temperature distributions to be obtained after the analyzes was compared with the experiments.

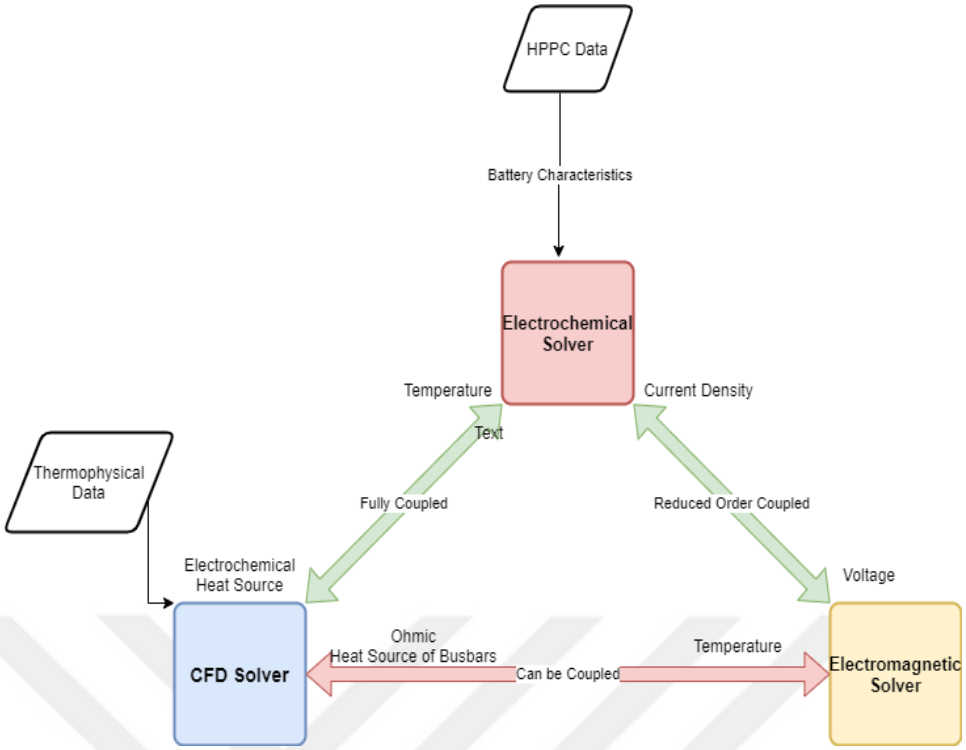

Figure 4.13. HPPC Data and Fluent Solver Chart [44]

In Figure 4.13, the roadmap to be followed for the analysis of battery packs is drawn. Electrochemical analysis is performed for the battery pack by using the test results obtained from the HPPC tests for the battery heat generation values required for the thermal analysis of the batteries. Obtained HPPC test data is added to Electrochemical analysis as battery data. HPPC test outputs at different temperatures and SOC values are loaded into Fluent in tables. With these experiments, the characteristics of the batteries were deduced. For the electrochemical analysis, the analysis setup preparation is completed together with the test results and the heat output values of each battery are obtained. These values are taken from the program as the heat generation per unit volume. The main output in electrochemical analysis is to determine the temperature values of the batteries.

After the heat outputs are obtained, the electrochemical analysis is terminated and the CFD thermal analysis part has started. The desired outputs in this section are the temperature values of each battery. Depending on these temperature values, changes are done in the design if necessary. The design has been changed at undesirable or above the limit temperature values. In addition, NTC sensor points are determined according to the temperature conditions.

In the CFD thermal analysis part, the conduction and convection heat transfer equations in the battery pack are solved as coupled. In addition, the thermal properties of the indoor and outdoor air are also included in the equations. Both solid volume and liquid volume are analyzed together. Conjugate heat transfer (CHT) analysis is performed.

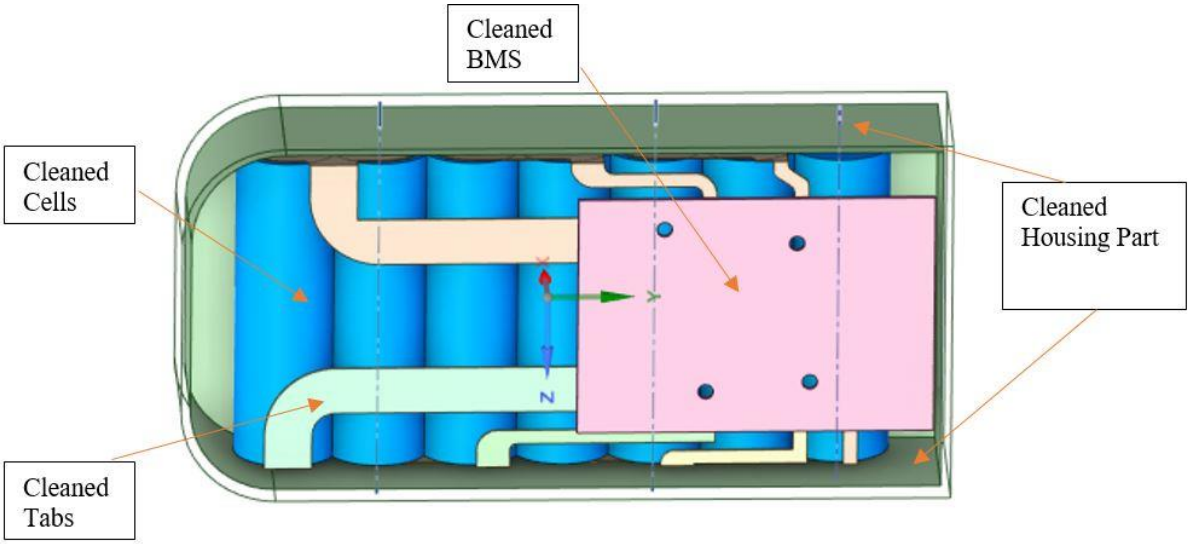

Figure 4.14. Vacuum Cleaner Battery and Housing Modelling

Figure 4.14 shows the vacuum cleaner battery after the cleaning process required for the analysis is done. In particular, all rounds in the cell holder that will not affect the analysis have been removed. In the outer housing part, arrangements have been made so that the internal air volume is preserved and optimization in the mesh number has been tried to be achieved. In the same way, the necessary cleaning processes are carried out on the tabs and batteries, and the geometry is ready for analysis.

Since two separate analyzes will be made, separate meshing and separate setup steps and result analysis were performed for each analysis. The meshing process for electrochemical analysis is as shown in the Figure 4.15.

Figure 4.15. Mesh Details for Electrochemical Analysis

In the electrochemical analysis, the current values passing over the batteries and tab materials were taken into consideration. For this reason, only batteries and tab materials were modeled and meshing was performed in the analysis study. As a result of the analysis, only the heat production values of the batteries were taken as output. Since the actual temperature rise values of the batteries will be revealed with the next thermal analysis, the temperature rise values were not considered in this analysis. Thus, there is no need to model the air volume inside the battery and the air volume outside the battery pack. In addition, the cell holder in the battery pack and the outer box of the battery pack were not included in the electrochemical analysis.

For the meshing process of batteries and tabs, 661997 polyhexcore cells were created. As a result of mesh processing, 37.5 aspect ratio was obtained as mesh quality. In addition, the minimum orthogonal quality value was found to be 0.2. Since the quality values obtained in the mesh process meet the mesh quality criteria, the setup part has been passed.

After the meshing process was completed, the setup part was started. Energy equations are activated as general solution settings. Transient solution method was chosen for the solution and convergence of the equations. The gravitational acceleration was entered in the appropriate direction and value to model the airflow correctly.

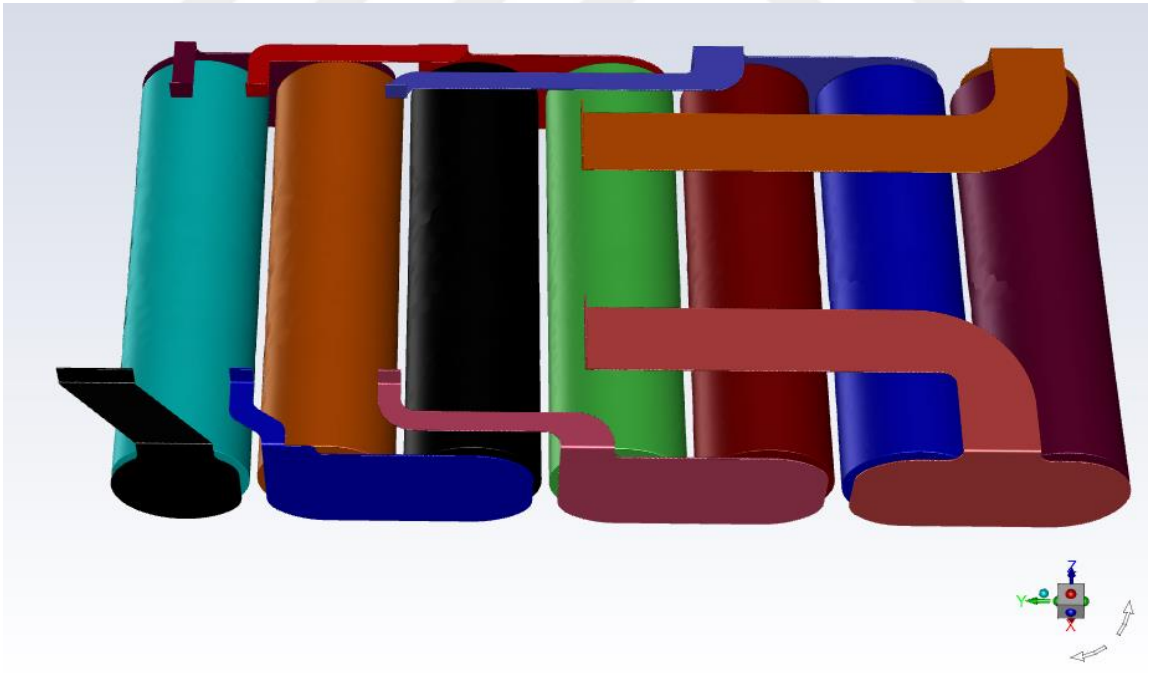

Figure 4.16. Electrochemical Analysis Setup

From the model options, the Battery Model solution is activated and the electrical requirements for the batteries in the battery pack are defined. MSMD was used as solution method and Equivalent Circuit Model was used for electrochemical model selection. A value of 1 was

entered as the C-rate. The minimum and the maximum stop voltage values are selected as 2.8 V and 4.3 V, respectively. In the conductive zone selections, batteries are selected as the active zone, while busbars and tabs are selected as the passive zone. Depending on the flow direction of the current, negative and positive tabs are introduced to the program. In the Model parameter section, we upload the battery data obtained from the individual battery experiments into Fluent in the appropriate format.

In the materials section, appropriate material data is defined for each component. The material of the batteries is defined as active material, and the material of tabs and busbars are defined as copper. Details on material information are shown in Table 4.5.

Table 4.5. Properties of Battery and Tab Material

	Material	
Properties	**Batteries**	**Tabs**
Raw Material	Lumped Parameter	Copper-Nickel Coated
Density (ρ) (kg/m^3)	2475	8978
Specific Heat (C_p) (J/kg.K)	1000	381
Thermal Conductivity (k) (W/m.K)	X — 3.3 Y — 3.3 Z — 15.0	387.6

The material information of the batteries and tablets can be seen in detail. As tab material, nickel-plated material on copper is used. Copper material was used to keep the temperature rises at low levels due to its high thermal conductivity and low thermal resistance. The reason for nickel coating on the copper material is to increase the laser welding capability of the tabs on the battery surfaces. In the material of the battery, the thermal conductivity coefficient, k, shows orthotropic properties. Therefore, while the thermal conductivity coefficient is 3.3 W/m. K in the cross-sections of the battery whereas it is 15.0 W/m. K in the longitudinal direction.

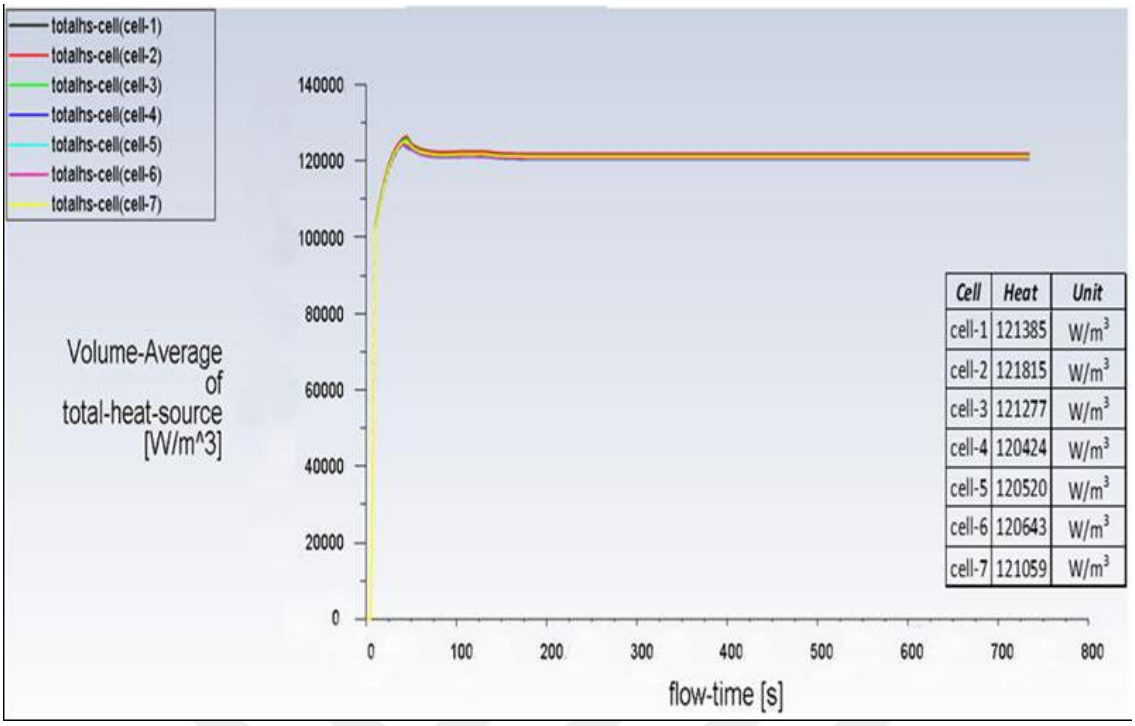

Figure 4.17. Electrochemical Result for Total Heat Source

In Figure 4.17, after the heat values in the electrochemical analyzes are obtained separately for each battery, the thermal analysis part is started. In this analysis, 1.2 x10^5 W/m^3 heat output per unit battery volume was obtained for each battery. These values were varied depending on the arrangement of the batteries. Since the individual temperature values of the batteries and their temperatures in the package will be determined in the thermal analysis, the entire battery pack is included in the thermal analysis modeling. The volume of the battery is 17204 mm^3. For this reason, the heat energy emitted from each battery was 2.08 W.

A heat generation value of 2.08 W was obtained for each battery from ANSYS Fluent HPPC analysis and HPPC experiments.

The thermal capacities obtained after HPPC experiments and analyzes were tried to be reached with analytical calculations. The aim here is to reduce all the experimental and analysis cost and to save time. For this reason, the internal resistance of the batteries was measured. The internal resistance value of the batteries was measured as 14 mΩ under room conditions. In discharge experiments, 12 A passes through each battery. Thus, the heat dissipated by a battery per unit time was calculated as in the equation below.

$$P_{heat-dissipated} = I^2 * R_{internal} \quad (4.1)$$

$$P_{heat-dissipated} = 12^2 * 0{,}014$$

$$P_{heat-dissipated} = 2{,}02\ W$$

While the heat production value of the battery was 2.08 W as a result of the experiment and analysis, it was 2.02 W in the analytical calculation. There is a difference of about 3% between them. This difference is thought to be due to the variation of the internal resistance of the heated battery with temperature.

After obtaining the heat output value for each battery, the CFD thermal analysis part is started. In this analysis, unlike the electrochemical analysis, the air volume and other solid components are also included in the analysis. Cover, cell holder and BMS components are also included in the analysis. The geometry of the cleaned vacuum cleaner geometry is shown in Figure 4.18.

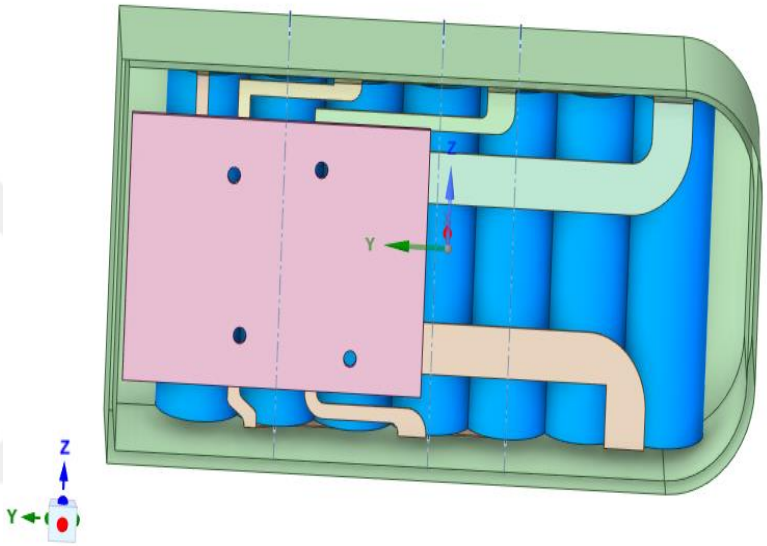

Figure 4.18. Cleaned geometry for CFD thermal analysis

Only the cleaned solid volumes are shown in Figure 4.18. In addition to solid volumes, the air inside and outside the box were also modeled in the analysis.

4.2.1.1. Mesh Study

After the geometry was created, modelling studies were carried out for three different mesh numbers in order to obtain a mesh-independent solution. Fluent mesh criteria were taken into account in all three mesh processes. Basically, element sizes were changed between mesh operations, and the frequency of transition mesh on thermal contact surfaces was changed.

Table 4.6. VC02 Mesh Dependency Study

	Mesh Details-1	**Mesh Details-2**	**Mesh Details-3**
Mesh type	Poly-hexcore	Poly-hexcore	Poly-hexcore
Cells	1288979	2089980	2603642
Cells per gap	1	3	3
Aspect ratio	60	43	58
Min orthogonal quality	0,19	0,2	0,17

In general, in CHT analysis, the number of elements in the contact regions should be at least 3 in order to better calculate the thermal transfers. For this reason, while a single element was used in the transitions in one mesh study, 3 elements were used in the other two analyses. The differences between mesh operations and the number of elements can be seen in detail in Table 4.6.

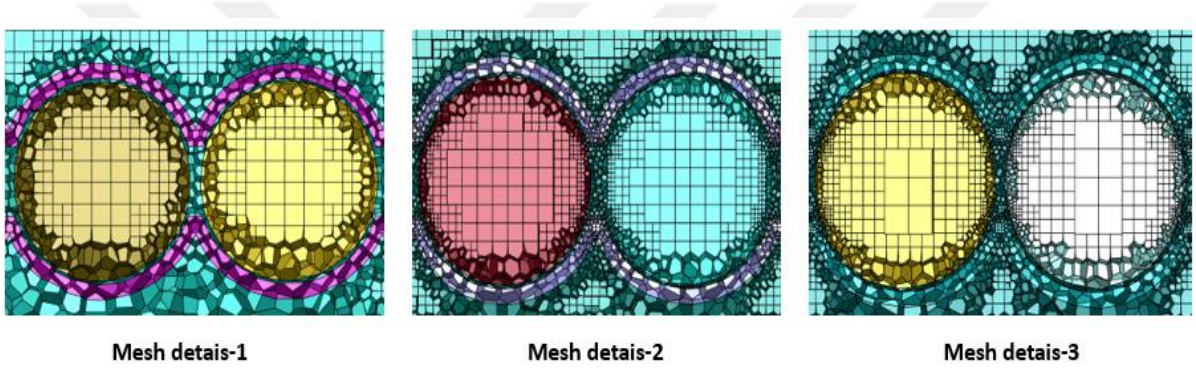

Figure 4.19. Cross-Sections of Transition Meshes Between Two Batteries

As can be seen in Figure 4.19, different mesh numbers have been studied in order to be able to accurately calculate the temperatures in the transition meshes between the two cells. Mesh densities have been increased and changes in heat transfer with convection to the indoor air have been tried to be seen. In addition, Fluent mesh criteria were provided in all mesh studies.

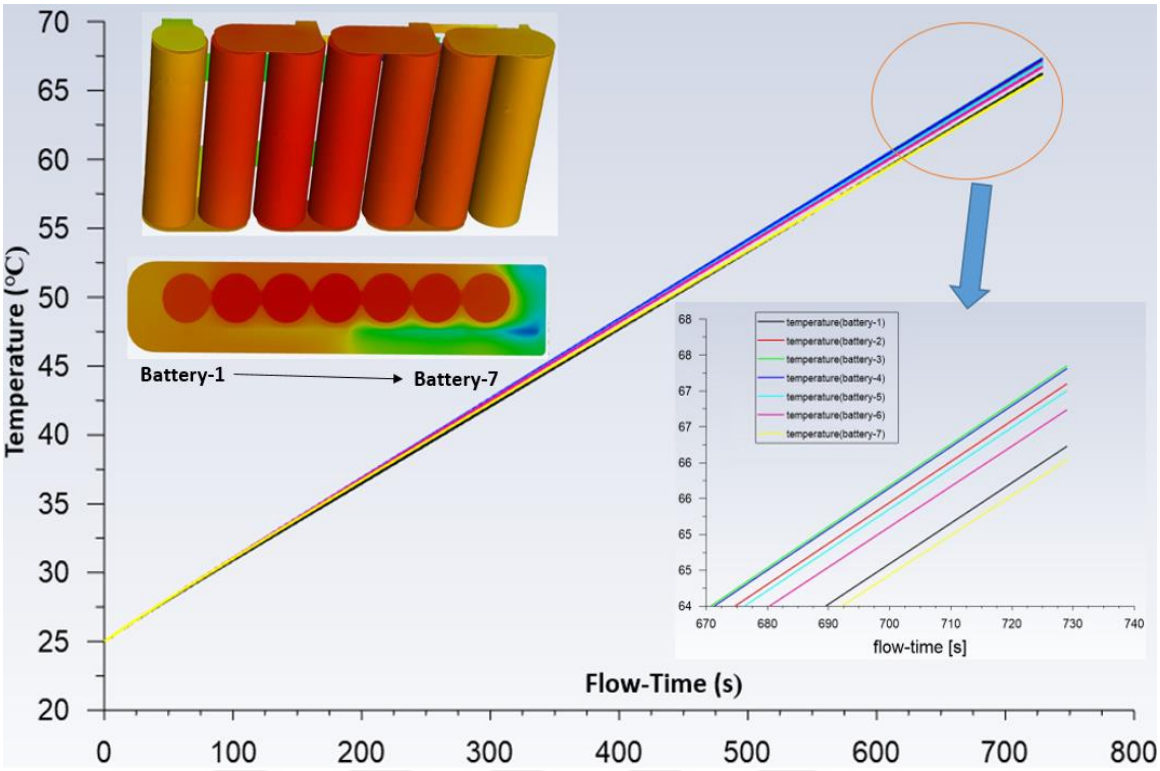

Figure 4.20. Thermal Results in First Mesh Study

The temperature contours taken from the battery pack and the temperature contours taken from the middle section of the batteries, the temperature graphs in the discharge analysis of the batteries are as seen in Figure 4.20.

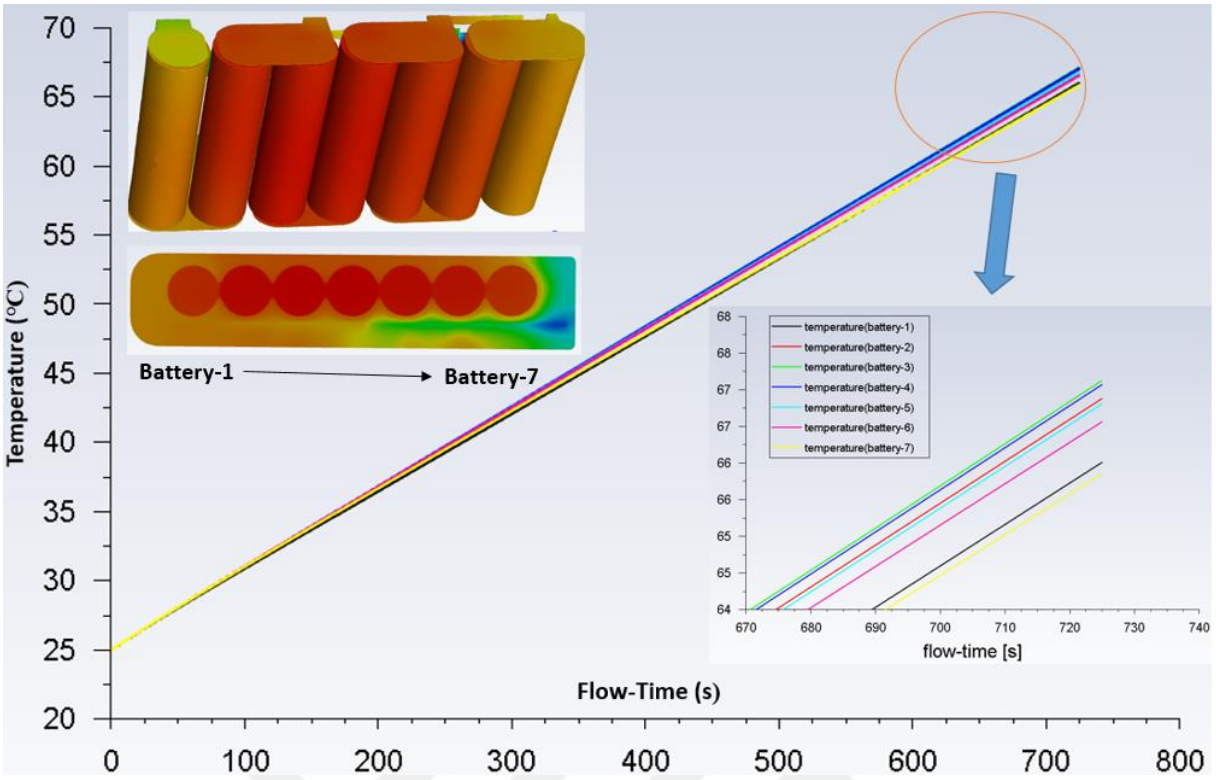

Figure 4.21. Thermal Results in Second Mesh Study

The temperature contours taken from the battery pack and the temperature contours taken from the middle section of the batteries, the temperature graphs in the discharge analysis of the batteries are as seen in Figure 4.21.

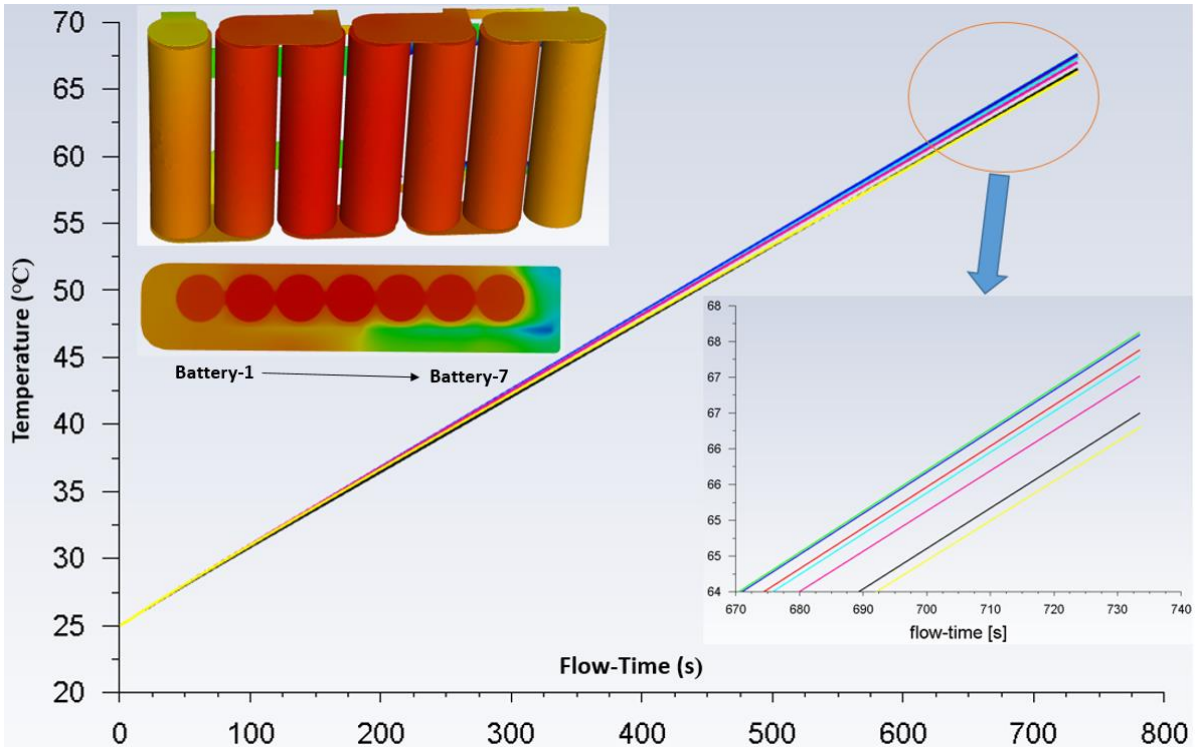

Figure 4.22. Thermal Results in Third Mesh Study

In all three mesh studies, the results are approximately the same as the Fluent mesh quality criteria are met. In the first mesh study, a single element was placed in the contact heat transfer zones, and the results were expected to be slightly different in this analysis. However, in solid volumes, especially in battery volumes, mesh density has enabled convergence values in solving equations. The contours and temperature graphs created to see the temperatures in the results section are consistent with each other.

Since the number of elements in the thermal contact regions recommended for CHT analyzes is three, the analyzes were continued with the second mesh study.

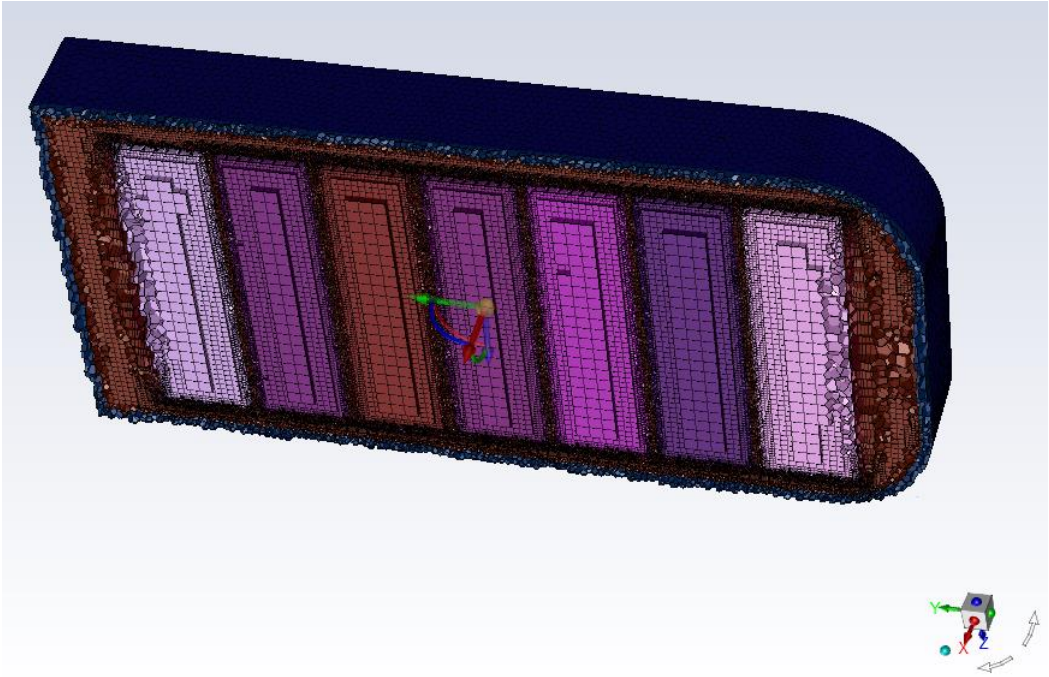

Figure 4.23. Solid and Liquid Volume Mesh Details

The mesh process for thermal analysis is as shown in the Figure 4.23. above. In the mesh process, 2,089,980 cell elements are used, of which 1,212,590 cells belong to the fluid volume and 877,390 cells belong to the solid volume.

In terms of surface mesh quality, the maximum skewness value that should remain below the 0.70 criterion was 0.59, and the maximum skewness value that should remain below the 0.9 criterion in volumetric mesh quality was 0.75. In addition, in the volumetric mesh quality control, the value of 0.1 was exceeded in the Orthogonal quality control that was found to be 0.2. As a result, the proposed criteria for mesh quality were provided for both surface meshes and volume meshes.

Table 4.7. Material Details of Solid and Liquid Components in Analysis

	Material			
Properties	**Batteries**	**Tabs**	**Cell Holder Cover**	**Air**
Material Details	Lumped Parameter	Copper-Nickel Coated	PC-ABS	Incompressible Ideal Gas Law
Density (ρ) (kg/m^3)	2475	8978	1125	
Specific Heat (C_p) (J/kg.K)	1000	381	1250	1006.43
Thermal Conductivity (k) (W/m.K)	X — 3.3 Y — 3.3 Z — 15.0	387.6	0.21	1.7894e-5

The material list and details of the parts used in the battery pack are shown in Table 4.7. The material of the outer housing and cell holder chamber is PC-ABS material, as Tab material, Nickel-plated material on copper is used. The air inside the battery is considered an ideal gas. The battery material is a special active material and the heat transfer coefficient is orthotropic. The transmission coefficient, which is the same in two axes, is different in the other axis.

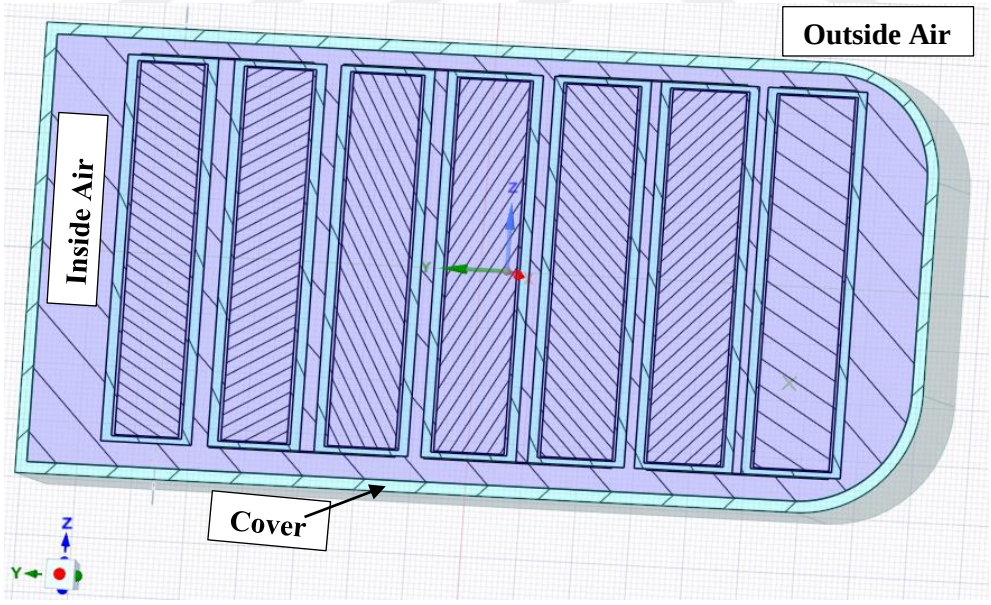

Figure 4.24. Thermal Conditions Inside and Outside the Battery Pack

The heat transfers in the battery pack are shown in Figure 4.24 and Table 4.8. While heat is transferred from the solid components in the battery pack by conduction, it is transferred from the solid components to the indoor air by convection. In addition, heat generation takes place in each battery. Heat transfer takes place by convection to the outside air over the cover.

Table 4.8. Thermal Conditions Inside and Outside the Battery Pack

No	Heat Generation and Transfer Mechanism
1	Heat transfer from inside the cover to the outside
2	Heat generation in batteries associated with 12 A discharge current
3	Heat convection in stagnant air inside

In Figure 4.24 and Table 4.8, heat transfer mechanisms and heat generation values in the battery pack are given. The fully charged battery is discharged at a current of 12 amps. In the analysis, the ambient temperature was accepted to be 25 °C. Considering the previous experiments, the heat transfer coefficient from the battery pack to the external environment was taken as 10 W/m^2K. Indoor air velocity was 0 m/s and natural convection analysis was performed.

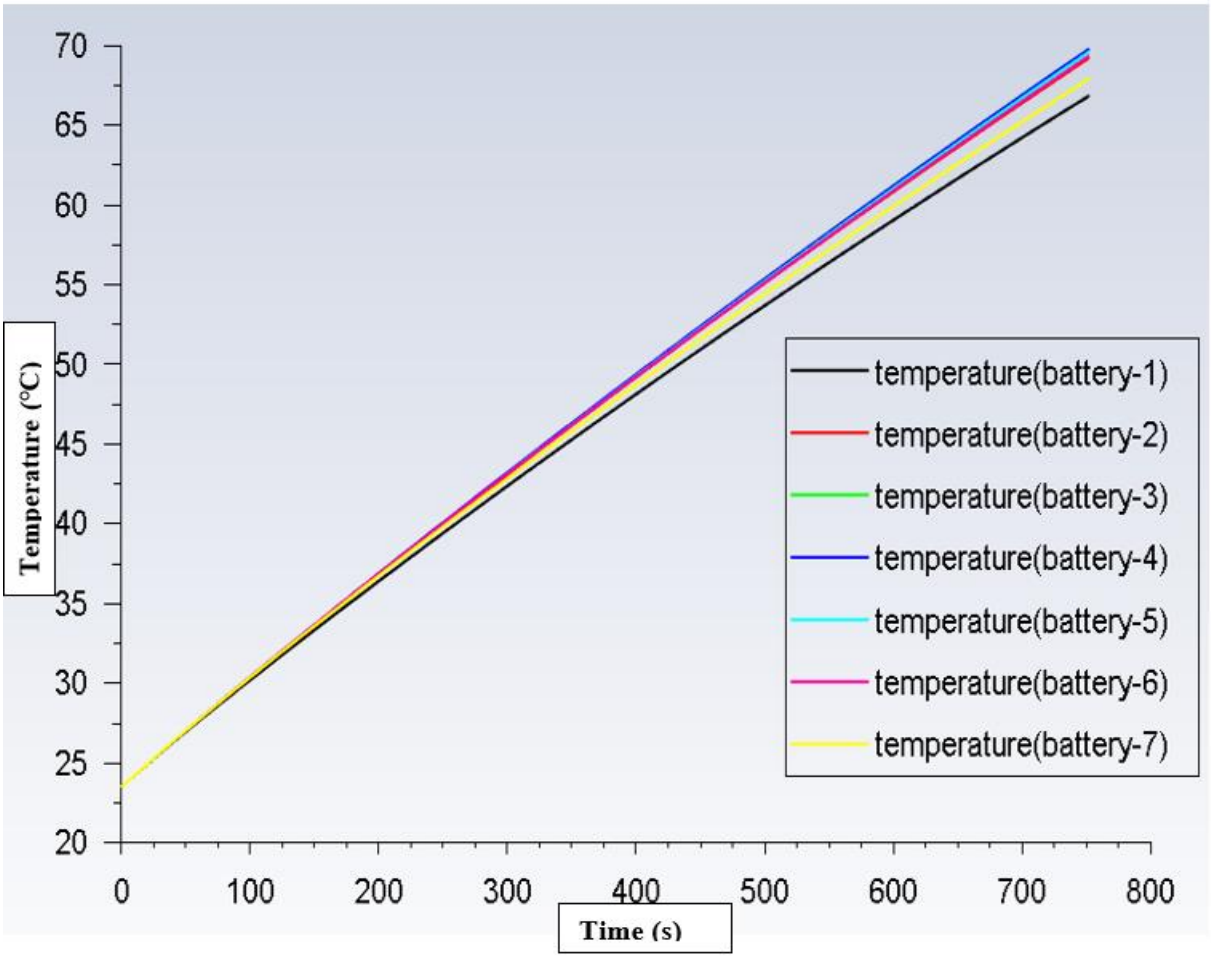

Figure 4.25. Temperature Distribution of Seven Cells

Figure 4.25 shows the temperatures inside the battery pack. Depending on the time, the temperature changes in the time until the fully charged batteries are discharged were found as in the figure. While the highest battery temperature was observed in the fourth battery in the volumetric averaged battery temperature results, close values were observed on the fifth and sixth batteries. The high temperature values can be observed especially in these batteries were

expected, where the air flow is low and they are under the BMS card. The lowest temperature values were observed in the first and seventh batteries on the side, where the air flow is higher and creates a better cooling effect.

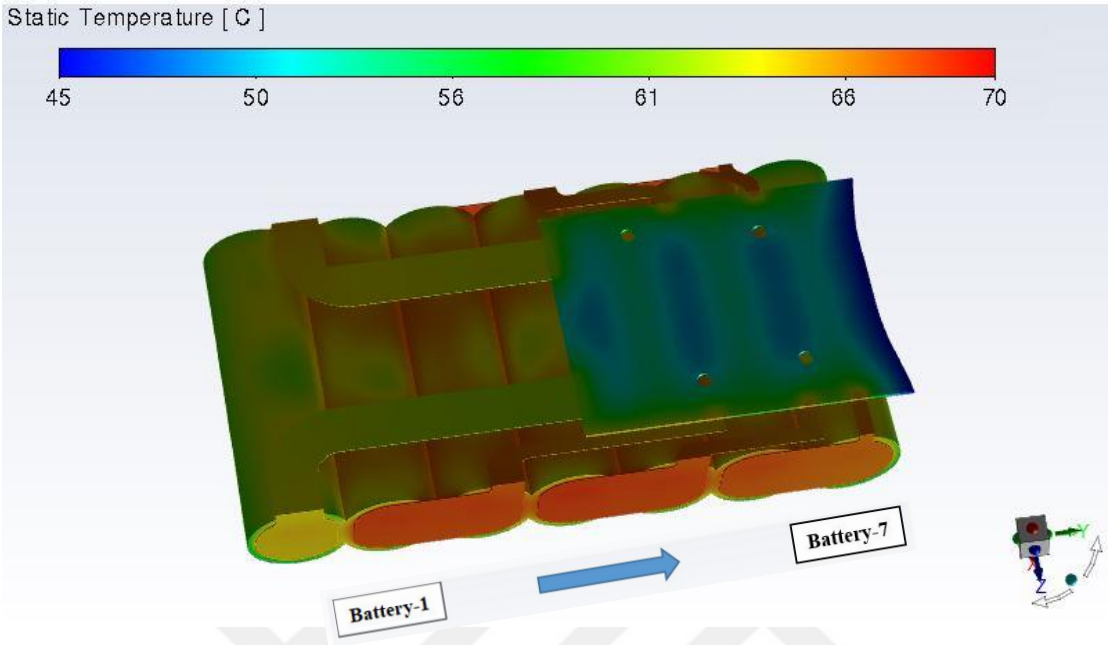

Figure 4.26. Temperature Distribution on Seven Batteries and BMS Card

As seen in Figure 4.26, temperature images from battery 1 to battery 7 are located from left to right. The battery with the coldest temperature values is the first battery. Afterwards, the coldest temperature value was seen in the seventh battery. The hottest batteries are the fourth and fifth batteries due to the least air flow.

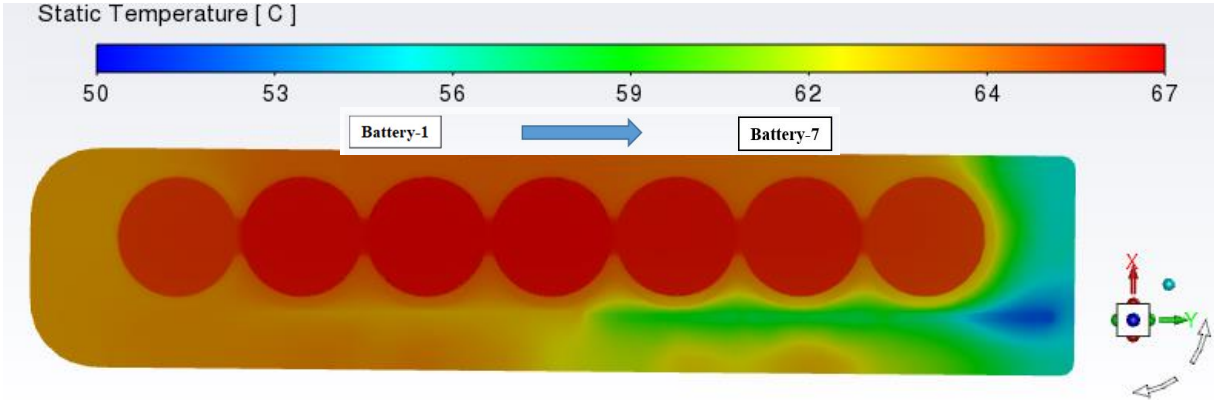

Figure 4.27. Cross-Sectional Image of Temperature Distributions Inside the Battery Pack

Figure 4.27 shows the cross-section of the temperature values taken from the battery surfaces. In this temperature distribution, the air flow inside the battery pack is also included. As can be seen in Figure 4.27, the temperature values are lower in the batteries on the edge, since the air

flow areas at the edges are more and it creates a cooling effect. The temperatures were higher in the batteries at the regions where the air flow is less.

4.2.2. Energy Storage System Design for Telecom Base Stations

Today's telecom networks are essential to consumers, public safety, and the economy which means system reliability is a top priority, even in off-grid or poor-grid situations typically found in emerging markets. 5G base station construction speed-up lithium iron phosphate market demand is bullish. Lithium iron phosphate batteries have high energy density and occupy less space than lead-acid batteries of the same capacity, providing greater convenience for the transformation of the original site 5G base station. The application of lithium iron phosphate energy storage equipment can also enable base stations to save electricity bills through power market transactions and applying peak-to-valley electricity prices to cut peaks and fill valleys.
The lithium-ion battery pack consists of 15 cells connected in series. Based on the thermal model developed for the single cell, the thermal behavior of the battery pack can be simulated and studied. The model of a typical 48 V 100 Ah L160F100 prismatic battery pack is shown in Figure 4.28 identical cells are modeled as two sets, one set of 7 batteries and the other set of 8 batteries. Adjacent pairs of batteries, series connection of batteries and electrical transmission are provided by 2 mm thick Aluminum busbar.

Figure 4.28. L160F100 Prismatic Cell

Figure 4.28 shows the image of a single battery with a prismatic structure. These are the busbar parts that transmit the electric current seen on the batteries. In this project, about 100 A current will flow through the batteries.
The geometric, electrical and thermal properties of the battery are given in the Table 4.9 below. In addition, the operating temperature ranges of the battery are as follows.

Table 4.9. L160F100 Prismatic Cell Technical Data [44]

Parameters of the Cell Characteristics and Geometry	
Quantity	**Value**
Rated capacity	100 Ah(RT, 1C/1C,2.5 3.6V)
Dimension (Length*Width*Height)	160× 49.9 × 118.4 mm
Mass energy density	162 Wh/kg
Volumetric energy density	338 Wh/L
Charging temperature	-5 to 55 ℃
Discharging temperature	-20 to 60 ℃
Max. uninterrupted charging/discharging current	100 A
Thermal management mode	Heating and Cooling

4.2.2.1. Heater Design for Charging

The heaters were analyzed individually before being analyzed in the entire battery pack. The analysis here was done to see how many degrees the heaters reach in the lean state. It has been observed whether these temperatures will cause problems in the contact of the heaters with other components in the battery pack. In addition, the heaters that were tested were compared with the analyzes. The thermal properties of the materials in the heaters were tried to be obtained.

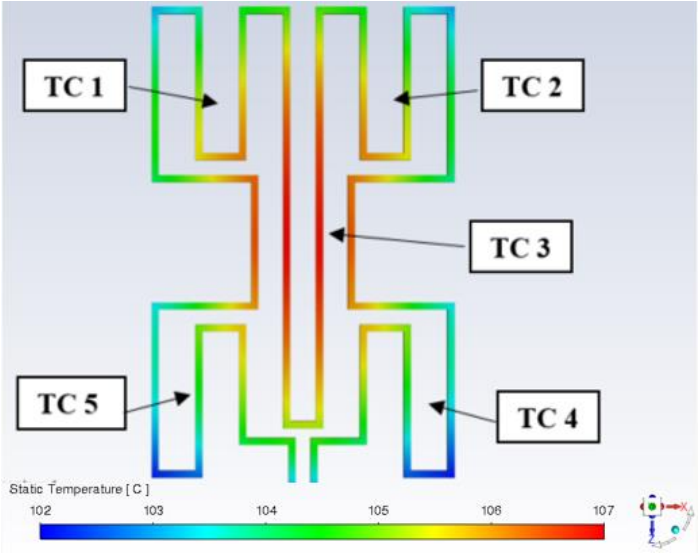

Figure 4.29. Temperature Distribution on the Heater

Figure 4.29 shows the temperature distributions on the heater. The abbreviation with TC stands for Thermocouple. The points selected here are set to be the same as the thermocouple points on the heater that was tested. As can be seen from the figure, while the temperatures around TC1, TC2 and TC3 points where the cables are heavily entangled, the temperatures seem higher, while around the TC4 and TC5 points, the circulation of the cables is less frequent and the temperatures are also lower.

Table 4.8. Temperature result of Thermocouple Points

TC1	106,1	℃
TC2	106,3	℃
TC3	106,9	℃
TC4	101,8	℃
TC5	102,6	℃

As seen in Table 4.8, the highest temperature was found as 106.9 C on Thermocouple number 3. Temperatures of around 106 C were detected on thermocouples 1 and 2. The lowest temperature was obtained from the number 4 and 5 thermocouples. The temperature value obtained from Thermocouple 4 is 101.8 °C. Thus, an acceptable difference of approximately 5 °C was found between the hottest and coldest surfaces. This value shows that the heat is ideally distributed on the surface in the preheater design. After these results obtained, the analysis of the heaters as a package was started.

In order for the battery packs used in telecom base stations to be able to charge properly, the batteries must be at suitable temperatures. Preheating may be necessary before charging, especially in battery packs used in low ambient temperatures. In the TBS project analysis, the minimum temperature requirement for charging the batteries is -5 ℃. It is aimed to bring the

temperatures raise up to -5 ℃ with the heater to be designed in cases where the temperature is lower. The heater control will be done via the BMS card. With the appropriate software, the heater will start to operate at ambient temperatures falling to -5 ℃, and then it will automatically stop working with the software when it comes to +5 ℃. Batteries that reach +5 ℃ will begin to charge.

The heater must bring the temperature of the batteries from -5 ℃ to +5 ℃ in a certain period of time for the charging process to start. This time period was determined as 45 minutes on average, taking into account the charging process. Since the desired heating capacities can be easily obtained by adjusting the number of windings and winding lengths, the foil type heater was chosen. Thermal analysis was carried out to determine the heating capacity to provide the required temperature conditions within the specified time.

a) Foil Type Heater **b)** Film Type Heater

Figure 4.30. Heater Types a) Foil Type Heater, b) Film Type Heater

The heater is designed to be embedded in the Cell holders in order to make the heat transfer to the batteries faster. While there is a PC+ABS material cell holder on the lower surface of the heater, there is a 1 mm thick Aluminum plate on the upper surface so that it can transfer heat to the batteries homogeneously.

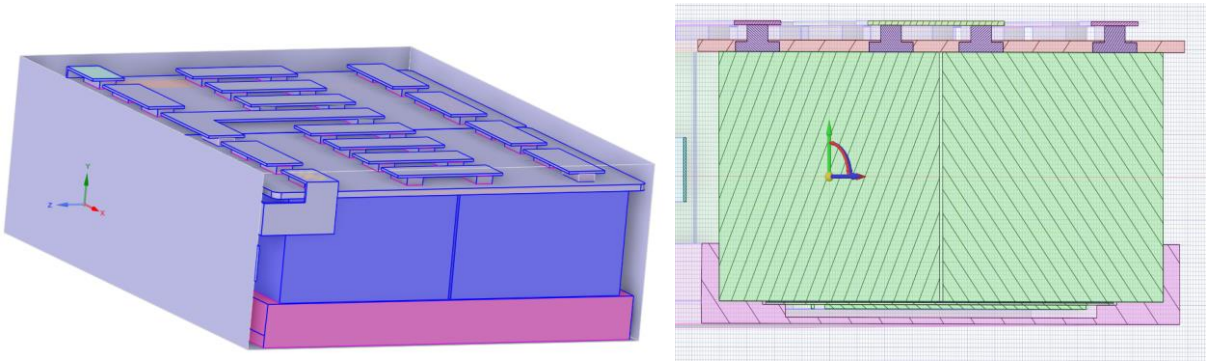

Figure 4.31. Model Geometry of Foil Type Heater and Battery Pack

The grid structure was created considering the mesh criteria. It was tried to increase the accuracy of the solution by using a dense mesh structure on the boundary surfaces where heat transfer will occur.

The meshing process for thermal analysis is as shown in the figure below. In the mesh process, 11,732,069 cell elements are used, of which 5,023,600 cells belong to the fluid volume and 6,708,469 cells belong to the solid volume. In terms of surface mesh quality, the maximum skewness value of 0.631, which should remain below the criterion of 0.7, and the skewness value of 0.836 in volumetric mesh quality, the condition of being below the criterion of 0.9 was met. With the volumetric orthogonal quality value of 0.16, the mesh quality criterion was met by being above the criterion of 0.10. As a result, the recommended mesh quality criteria for both surface meshes and volume meshes were provided.

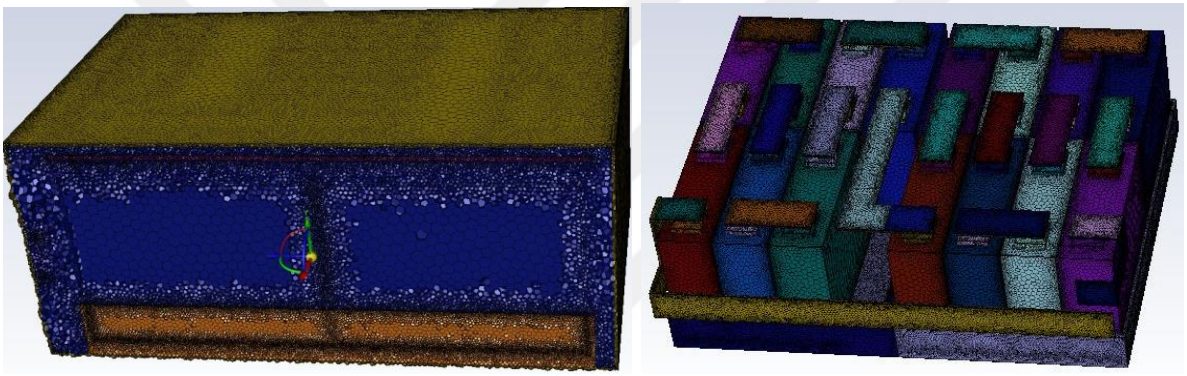

a) **b)**

Figure 4.32. Mesh Details of Battery Pack and Heater, a) Front View, b) Isometric View

The mesh structure is shown in Figure 4.32. In Figure 4.32a, there is an image of the solid volume together with the air volume, and we can also name it as Full volume mesh. Figure 4.32b shows only the solid volume. All parts and models that were valid and effective in thermal analysis were meshed.

The material list and details of the parts used in the battery pack are shown in Table 4.9. The material of the outer casing is steel. The cell holder material is PC-ABS, as Tab material, Aluminum is used. The air inside the battery is considered an ideal gas. The battery material is a special active material and the heat transfer coefficient is orthotropic. The conduction coefficient, which is the same in two axes, is different in the other axis.

Table 4.9. Material Details of Solid and Liquid Components in Analysis

	Material					
Properties	**Batteries**	**Tabs**	**Cell Holder**	**Cover**	**Heater**	**Air**
Material Details	Lumped Parameter	Al 1050	PC-ABS	Steel	Chromium Nickel	Incompressible Ideal Gas Law
Density (ρ) (kg/m^3)	2104	2820	1125	8030	8900	
Specific Heat (C_p) (J/kg.K)	1086	900	1250	502.5	461	1006.43
Thermal Conductivity (k) (W/m.K)	X — 19.83 Y — 19.83 Z — 1.13	202	0.21	16.3	91.7	1.7894e-5

The heater is analyzed for different capacities when it is in the off position without charging or discharging on the battery pack. The heater supply will be 24V. The electricity supply that will come through a single connector will be divided into two battery groups.

The heater works as a heat source inside the battery pack. In addition, the air in the battery pack provides a natural convection effect. Heat is transferred from the battery pack to the outside air. Considering all these heat transfer mechanisms, boundary conditions were created and defined in the analysis. In addition, it was assumed that there was no air flow in the battery pack at the beginning. At the beginning of the analysis, the ambient temperature was accepted as -5 ℃.

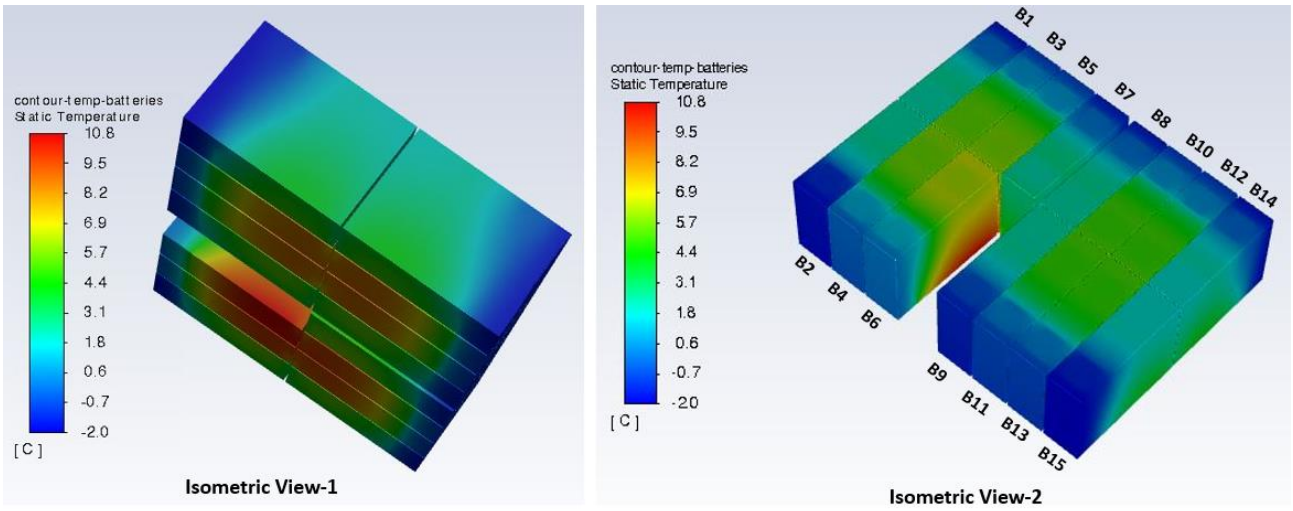

Figure 4.33. Temperature Distributions on Battery Surfaces After 120W Capacity Analysis

The first seven batteries are named as battery group 1, and the next 8 batteries are named as battery group 2. Identical heaters are used for both battery groups.

Figure 4.33 shows the temperature distributions on the battery surfaces after the 120 W analysis.

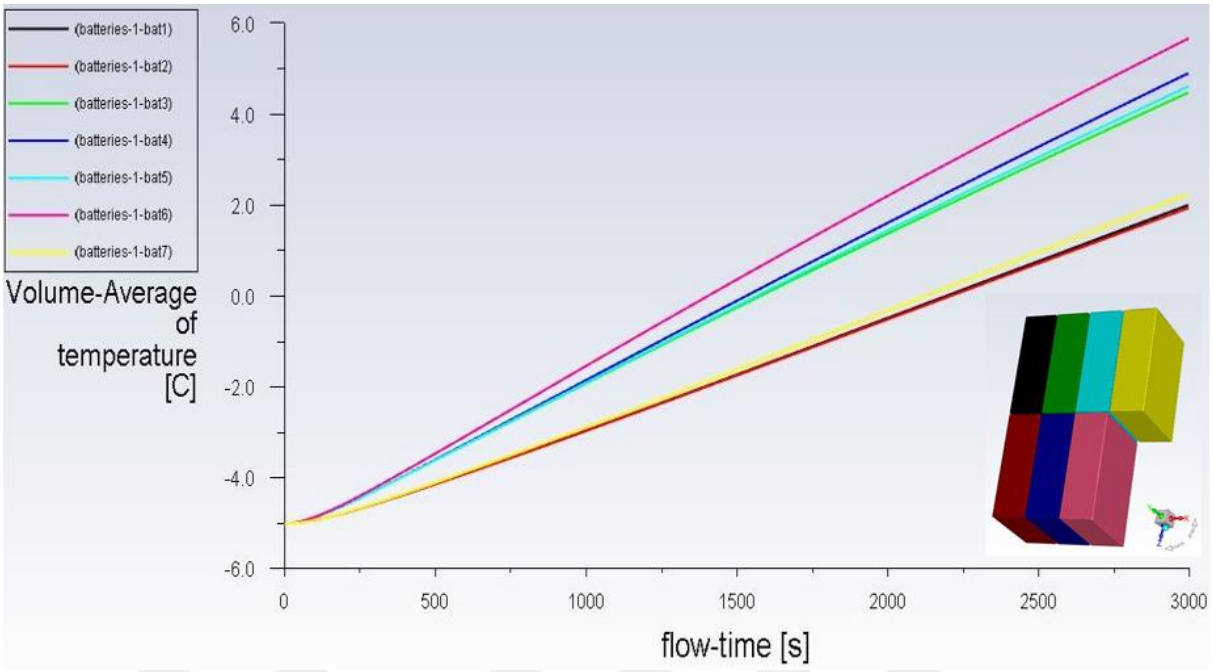

Figure 4.34. Volume Averaged Temperature Values for Battery Group 1 at 60W Capacity

Figure 4.34 shows the volumetric temperature averages of the 7 batteries in the first battery group as a result of the thermal analysis. The positions of the batteries on the graph can be understood from the visual in the lower corner of the graph. The color of each battery on the graph and the color scale in the image are identical. In general, and as expected, the temperature averages were higher for the batteries that took up more surface space on the heater, while the temperature averages were lower for the batteries that took up less space on the heater.

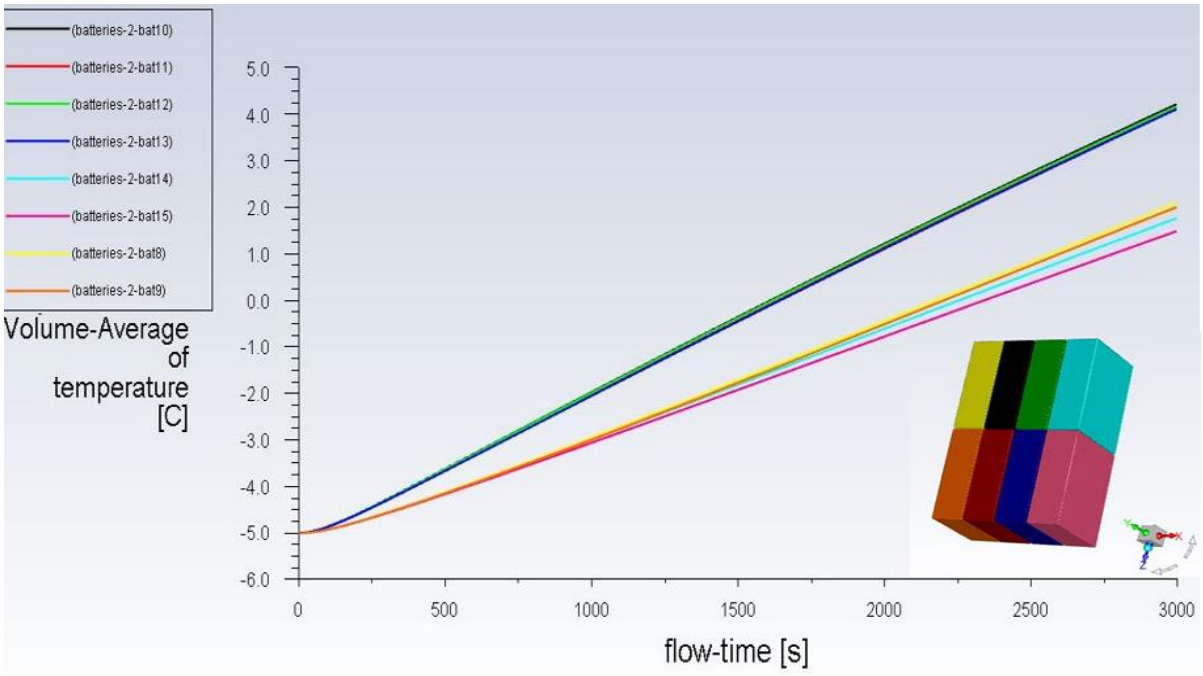

Figure 4.35 Volume Averaged Temperature Values for Battery Group 2 at 60W Capacity

Figure 4.35 shows the volumetric temperature averages of the 8 batteries in the first battery group as a result of the thermal analysis.

4.2.2.2. Cooling Design for ESS Battery Pack

Within the scope of the ESS project, a cooler design study has been carried out so that the battery pack can operate in the appropriate temperature range. Before starting the cooling design calculations and analysis, all heat generating components in the Front Panel section were identified. According to the results obtained from previous performance tests, it was seen that the batteries do not heat up to high temperatures. Therefore, electronic components on the PCB are included in the calculations in order to obtain the results faster in the cooler fin design study. All components and heat sources that play an active role in heat transfer are included in the calculation.

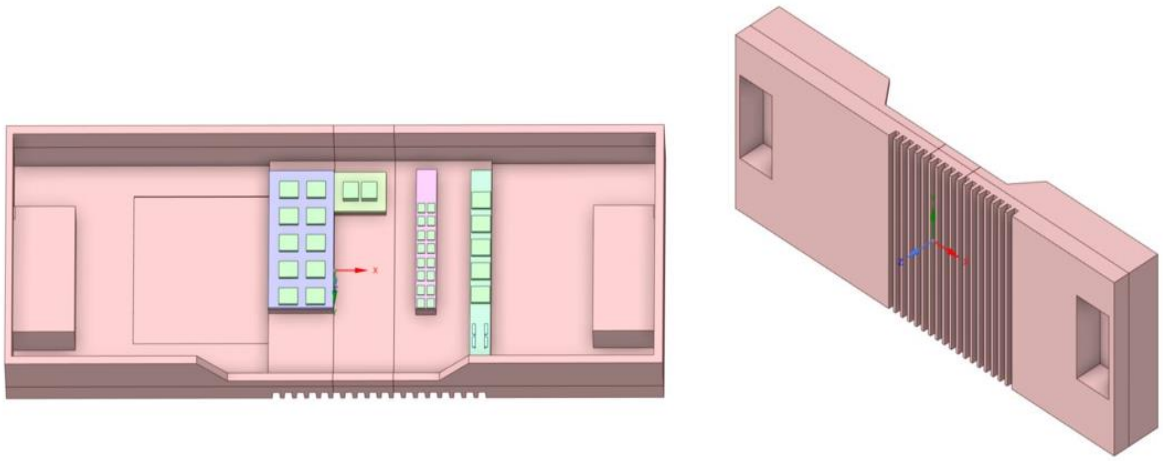

Figure 4.36. Aluminum Heat Sink and Electronic Components

There are 31 Mosfets, 2 Sense Resistors and 2 Diodes placed on the PCB. On the other side of the electronic components, there is a thermal gap filler material to increase heat transfer. Thermal gap fillers were adhered to the areas on the Al heat sink. Thus, the heat generated in the electronic components is transferred to the Al heat sink over the thermal gap fillers in the direction of the PCB and cooled.

Analytical calculations were first started by calculating the heat produced by each component.

Table 4.10. Thermal and Material Properties of Electronic Components

Components	Density (kg/m^3)	Specific Heat (J/kg.K)	Thermal Cond (W/m.K)	Resistivity (mΩ)	Current (A)	Capacity per Component (W)
Mosfets-1	2390	7120	150	6	8	0.38
Mosfets-2	2390	7120	150	5	20	2.00
Diodes	2390	6000	190	4.3	25	2.69
Sense Resistance	2650	300	200	1	50	2.50

Table 4.10 above contains the material and thermal properties of all electronic components on the PCB. The current passing through the battery pack is 100 Amperes. The current values passing through each electronic component and the internal resistivity values of the components are as shown in the table. The electrical capacity calculation made according to the current values and internal resistances passing through it is as follows.

$$q = I^2 * R \tag{4.2}$$

The heat generation values for each component were calculated according to the above equation 4.1. The heating values found for each component were then multiplied by the number of components and the total heat production value in the Front Panel was found.

Table 4.11. Total Heat Capacity of Components

Components	Counts	Unit Heat (W)	Total Capacity (W)	Tolerans (%)	Total Capacity with Tolerance (W)
Mosfets-1	16	0,4	6,4	20	7,7
Mosfets-2	15	2,0	30,0	20	36,0
Diodes	2	2,7	5,4	20	6,5
Sense Resistance	2	2,5	5,0	20	6,0

The heat generation values on the PCB originating from electronic components are as shown in Table 4.11. Internal resistance values increase with increasing temperature. However, since we could not reach this value from the tables, 20% was added to the thermal capacities in order to include the extra internal resistance increase due to the temperature increase in the calculations.

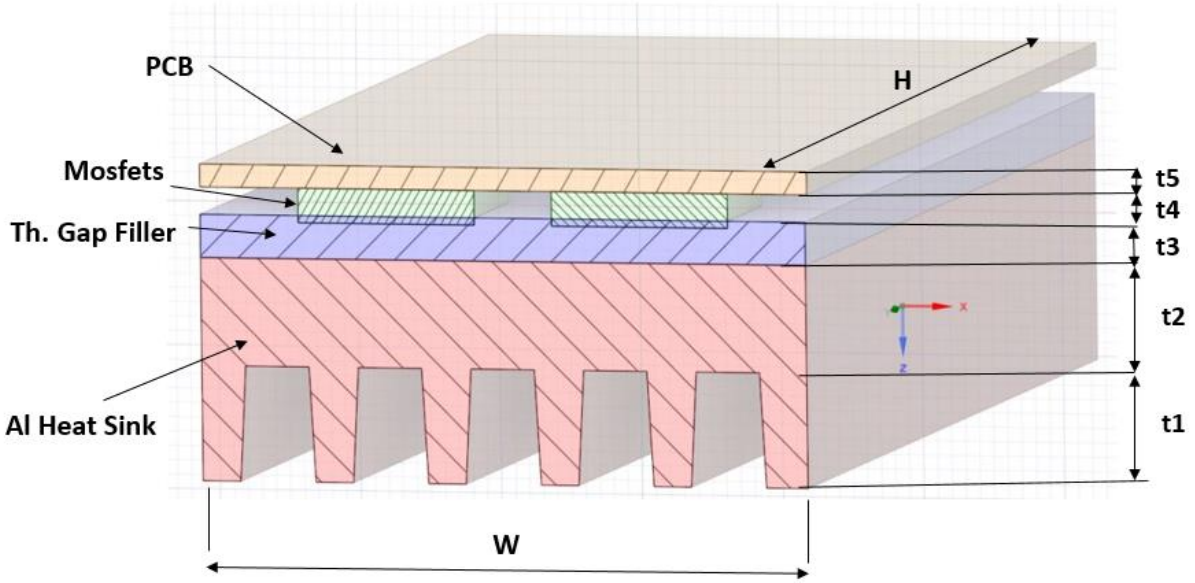

Figure 4.37. Cross Section of Thermal Resistance

After calculating the heat production values of the electronic components, the regional temperature changes were calculated by separating the sections with the components using the thermal resistance method.

The heat emitted from the components is conveyed in the direction of the PCB and the direction of the Al Heat Sink. There is also heat transfer from electronic components to air by convection. Since it is operated at low temperatures and the temperature differences are very low, heat transfer by radiation has been ignored in the calculations.

The following thermal resistance method was used to calculate the heat transfers by conduction and convection.

$$\begin{pmatrix}\text{Rate of heat transfer}\\ \text{into to the wall}\end{pmatrix} - \begin{pmatrix}\text{Rate of heat transfer}\\ \text{into to the wall}\end{pmatrix} = \begin{pmatrix}\text{Rate of change of the energy}\\ \text{of the wall}\end{pmatrix} \quad (4.3)$$

$$\dot{Q}_{cond,wall} = kA\frac{(T_1 - T_2)}{L}\ (W) \qquad \dot{Q}_{conv} = hA_s(T_s - T_\infty)\ (W) \quad (4.4)$$

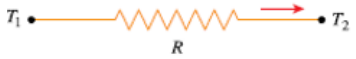

$$\dot{Q}_{cond,wall} = \frac{T_1 - T_2}{R} \qquad \dot{Q}_{conv} = \frac{T_s - T_2}{R_{conv}} \quad (4.5)$$

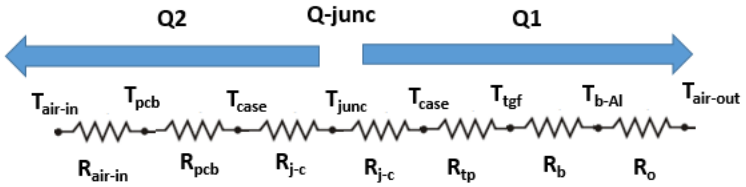

Table 4.12. Thermal Resistance and Max Temperature Limit of Electronic Components

Components	Thermal Resistance junction-case (°C/W)	Thermal Resistance junction-ambient (°C/W)	Max Temperature (°C)
Mosfets-1	0.5	42	175
Mosfets-2	0.34	40	160
Diodes	2.5	34	150

Substituting the thermal resistance values in Table 4.12 in the equations 4.4 above and solving all the thermal resistance equations together, the following results are obtained.

Each Mosfets group is included in separate accounts. Accordingly, the thermal pad, PCB and Al heat sink area are included in the calculations to have the same area. The thermal resistance value of each material was calculated and then the total resistance value was found. The thermal resistance results prepared for the sections shown in Figure 4.37 are as shown in the Table 4.13 below.

Table 4.13. Thermal Resistance of each Component

Resistances	Value	Unit
R_{tgf}	0.199	K/W
R_{Al}	0.005	K/W
$R_{air,o}$	2.324	K/W
R_{PCB}	0.213	K/W
$R_{air,i}$	26.578	K/W
$R_{sum,1}$	2.528	K/W
$R_{sum,2}$	26.791	K/W

After the thermal resistance values have been calculated, the value of each component is substituted into the heat equation 4.4. Outdoor temperature is assumed to be 20°C.

Table 4.14. Temperature Results for Mosfets and Air

Thermal Output	Value	Unit
$T_{air\text{-}in}$	41	°C
$T_{air\text{-}out}$	20	°C
$T_{junction}$	86,5	°C
Q_1	22,55	W
Q_2	1,46	W
Q_{sum}	24,00	W

Table 4.14 shows the temperatures and total cooling capacity obtained as a result of analytical calculations. Each Mosfets emits 2.4 W of heat energy. 10 Mosfets of the same type were used

in the area included in the calculation. Thus, the amount of heat emitted from the Mosfets throughout the entire area is Q_{in}=24W. In the analytical calculations, first of all, thermal resistance values were calculated for two separate heat transfers. The heats of Q_1 and Q_2 transferred over these two paths will be equal to the heat emitted by the Mosfets when the system reaches thermal equilibrium. Therefore, the sum of the heats of Q_1 and Q_2 is taken as 24W. When substituted in the heat equation, the unknowns are only the temperature of the indoor air and the temperature of the Junction region of the Mosfets. The indoor temperature was accepted within the results obtained from the experiments. The temperature of the Mosfets was obtained in the solution of the equation. As a result, the Mosfets temperatures were found to be 86°C using analytical calculations.

As a result of the thermal analyzes made in Fluent, the temperature of each battery and the temperature distributions in the heat sink area were obtained. The determination of the hottest and coldest batteries and verification by experiments were carried out. In addition, the temperatures on the front panel side were determined regionally. The temperature distributions in the Mosfets and the temperatures in the contactable zone on the outer surface of the heat sink were found.

Analyzes were performed under the same conditions and initial conditions for comparison with the experiments. Therefore, the ambient temperature was taken as 20 °C. The heat dissipation capacities of each battery and electronic components are defined. Solver settings in heat transfers in the battery pack were adjusted in accordance with CHT analysis. Thus, both the

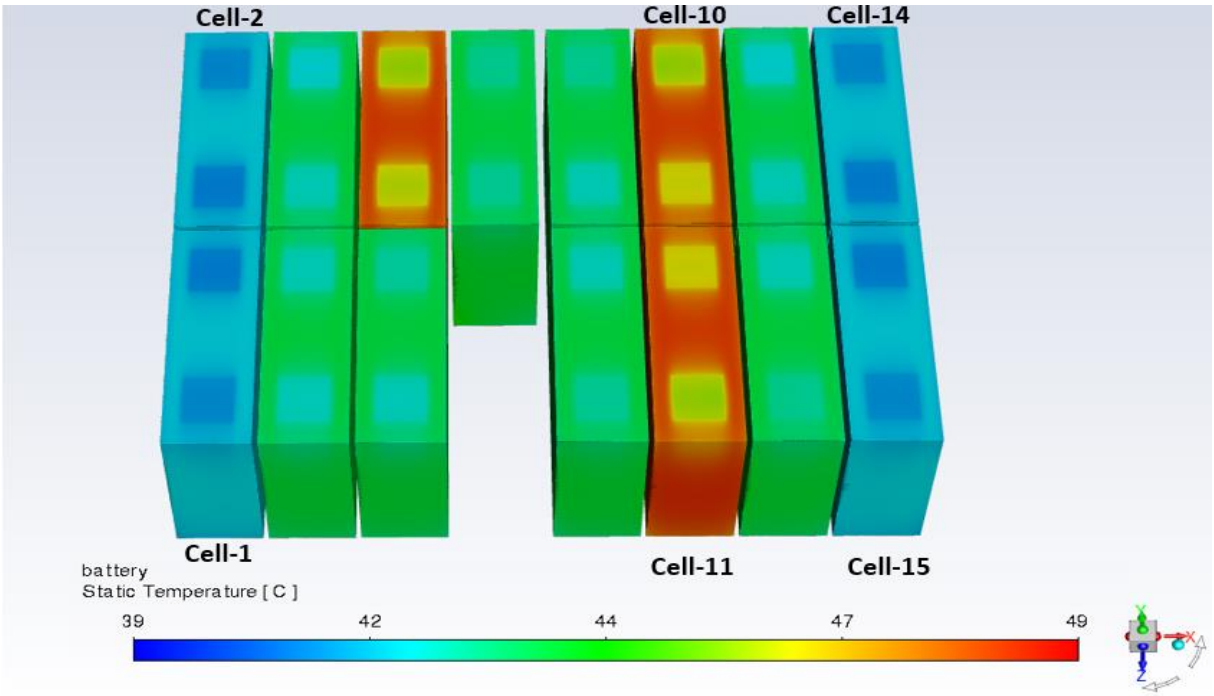

Figure 4.38. Thermal Discharge Analysis of ESS Battery Pack

convection and the conduction equations are derived to be solved together in a transient manner. In addition, the ambient air, outside the battery pack, is modeled to calculate the heat transfer from the outer cover of the battery pack to the environment. During the discharge experiment, a current of 100 A passed through each battery.

As a result of the thermal analysis, the hottest batteries were seen in the areas where the air circulation is the least and therefore the convection coefficient is the lowest. On the other hand, the batteries with the lowest temperature were observed on the batteries on the edges, where the air circulation is more and the convection coefficient is higher.

As seen in Figure 4.38, the highest temperature values were reached in battery 10, battery 6 and battery 7. Temperatures in these batteries were 48.1 °C. The lowest temperature values were seen in battery 1, battery 2, battery 14 and battery 15 located on the edges of the battery pack. The temperatures on these batteries were found to be 41.9 °C. Thus, the maximum temperature difference between the hottest batteries and the coldest batteries is 6.2 °C.

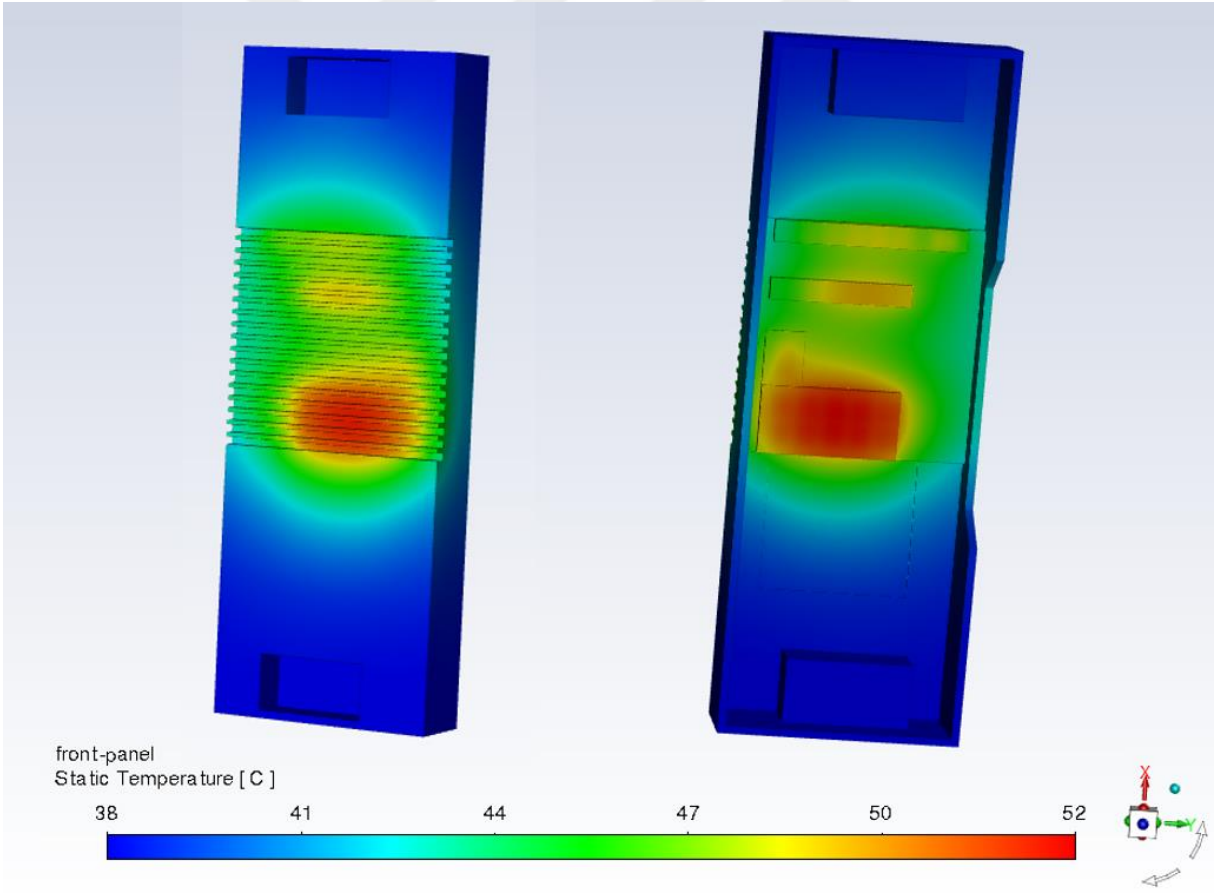

Figure 4.38. Temperature Distribution of Al Heat Sink

Cooling analysis was performed on the battery pack. Figure 4.39 shows the temperature distribution on the Al Heat sink. The detailed temperature distribution of the heat sink in the

indoor and outdoor directions is as shown in the figure. The maximum temperature value obtained on the fins on the outer surface is 51.5 ℃.

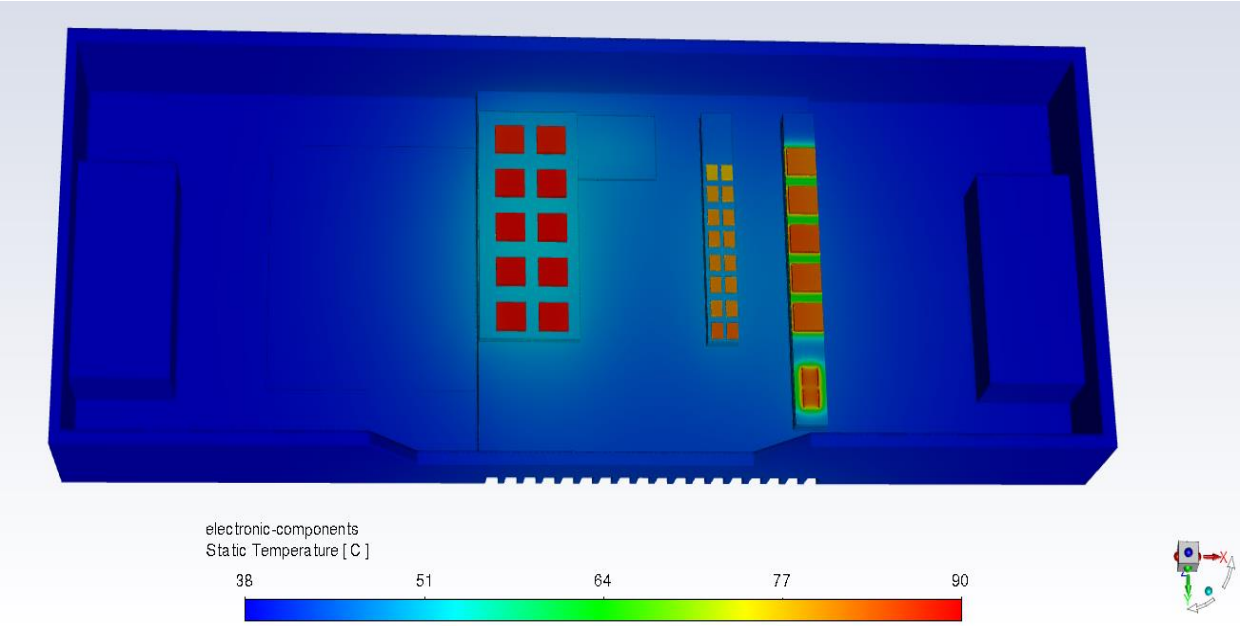

Figure 4.39. Temperature Distribution of Electronic Components

Temperature distributions on electronic components can be seen in Figure 4.40. The temperature outputs of two different Mosfets group and one sense resistance were obtained. The highest temperature values were seen in MDT type Mosfets, which is the component considered in analytical calculations. The maximum temperature value seen in these electronic components is 89.5 ℃.

Both the temperature value in the contactable areas on the outer surface of the external heat sink and the temperature value on the electronic components remained at an acceptable level. In addition, since the surface areas of electronic components are very small compared to PCB and heat sink, their temperature impact areas are very limited.

5. CONCLUSIONS

In this thesis, the modeling of batteries with the ANSYS Fluent program was studied. As a validation study, an analysis study of a vacuum cleaner battery with seven cylindrical batteries was performed at the beginning. First, single HPPC experiment was performed on the batteries and variation of voltage and current values with SOC at different ambient temperatures were plotted. Results from this experiment were transferred to the ANSYS Fluent Electrochemical Analysis run. As a result of this analysis, the thermal capacity values of each battery were obtained. Thus, the heat capacity of each battery per unit time was obtained. This thermal capacity value was used as the thermal input in the next Fluent thermal analysis. All solid volumes and indoor and outdoor air were modeled in Fluent thermal analysis. As a result, the temperature outputs of each battery were found separately. Experiments of the battery pack modeled in the analysis study were carried out in thermal cabinets under the same conditions. Afterwards, the results of the analysis and the results of the experiment were compared and their comparison with each other was revealed.

When the temperature results obtained in the experiments were compared with the numerical analysis results, it was seen that the batteries with the maximum and minimum temperatures were found correctly. In addition, it was understood that the temperature value of the batteries with the maximum temperature was the same as the experiments. Observed as a difference, the temperature of the battery with the lowest temperature was found to be 2.5 ℃ higher in the analyzes compared to the experiments. As a result of this, while the maximum temperature difference was 6.0℃ in the experiments, the analyzes were 3.5℃. It is thought that this difference is due to the fact that the actual thermal properties of the materials may differ slightly from the catalog values and that it creates some difference in thermal transfers due to ideal air assumption.

After the verification work on cylindrical batteries, Telecom Base Station battery studies were carried out to be used in the more complex ESS project. 15 prismatic batteries were used in this project. In addition, pre-heating design and cooling design were made in this project. The preheater was designed to ensure that the batteries reach the required temperature for charging at low ambient temperatures. With the necessary analysis studies, transitions were provided with Al plate so that the heat emitted from the heater can be optimally distributed through the batteries. In addition, the heater channels are effectively distributed on the surface, facilitating the transfer of heat from the center to the edge surfaces.

In addition, thermal discharge analyzes and experiments were carried out for the TBS battery pack. In analyzes and experiments, the hottest and coldest batteries were found at the same locations. While the hottest battery reached 50 ℃ in the experiments, the same battery was seen as 48 ℃ in the simulations. The coldest battery was 44.5 ℃ in the experiments, it was seen as 43.5 C in the numerical analysis. As a result, while the locations of the hottest and coldest batteries were determined correctly, some quantitative differences were observed between the temperatures. Apart from this, the maximum temperature difference was found to be 4.5 ℃ in the analyzes and 5.5 ℃ in the experiments. When all the results are evaluated, it is seen that the results are in good agreement.

Finally, in this project, a battery cooling design was done in order to prevent temperature increases caused by the heat generated by electronic components. The heat produced by each component was determined and then the Al heat sink was designed. The temperatures on the components and on the outer surface were analyzed. In addition, analytical calculations were performed on the determined control volume and the appropriate design was decided. In order to reduce the number of analyzes, the parameters in the analytical calculations were reduced and finally the project we completed with numerical studies.

6. REFERENCES

[1] British Petroleum, (2016), “BP statistical review of world”, Energy.

[2] British Petroleum, (2016), “BP Energy Outlook 2016”, 53.

[3] Andersen PH., Mathews JA., Rask M., (2009), „“Integrating private transport into renewable energy policy: the strategy of creating intelligent recharging grids for electric vehicles““, Energy Policy, 37, 2481–2486.

[4] Saleh, S. A., “An Investıgatıon On the Comparıson of the Performance of Lıthıum-Ion Batterıes and Nıckel Metal Hydrıde Batterıes Used in Electrıc Vehıcles”, Master Thesis, Karabuk University, Karabuk, Turkey, (2021).

[5] Greco, Angelo. Numerical and analytical modelling of battery thermal management using passive cooling systems. Lancaster University (United Kingdom), 2016.

[6] Väyrynen A., Salminen J., (2012), „“Lithium ion battery production““, J Chem Thermodyn, 46, 80–85.

[7] Pesaran A, Santhanagopalan GK., (2013), „“Addressing the impact of temperature extremes on large format Li-ion batteries for vehicle applications.

[8] Motloch CG, Christophersen JP, Belt JR, Wright RB, Hunt GL, Sutula RA, et all., (2002) „“High-power battery testing procedures and analytical methodologies for HEV“s““, Future Car Congress, 1–7.

[9] Pesaran Aa., (2002) „“Battery thermal models for hybrid vehicle simulations““, J Power Sources, 110, 377–382.

[10] Dahn, J., & Ehrlich, G. M. (2011). Lithium-ion batteries. In T. B. Reddy (Ed.), Linden’s handbook of batteries (pp. 26.1–26.79). New York: McGraw-Hill.

[11] Park, J. (2012). Principles and Applications of Lithium Secondary Batteries, Engineering Pro collection, Wiley, https://books.google.com.tr/books?id=papHHurMVYC.

[12] N. H. F. Ismail, S. F. Toha, N. A. M. Azubir, N. H. M. Ishak, M. K. Hassan och B. S. K. Ibrahim,” Simplified Heat Generation Model for Lithium-ion battery used in Electric Vehicle.,” International Conference on Mechatronics (ICOM'13), Kuala Lumpur, 2014.

[13] Andrea, D. (2010). Battery Management Systems for Large Lithium Ion Battery Packs, EBL-Schweitzer, Artech House, https://books.google.com.tr/books?id=o-QpFOR0PTcC.

[14] Farag, M.S. (2013). Lithium-Ion Batteries: Modelling and State of Charge Estimation, 169.

[15] Espedal, I.B.; Jinasena, A.; Burheim, O.S.; Lamb, J.J. Current Trends for State-of-Charge (SoC) Estimation in Lithium-Ion Battery Electric Vehicles. Energies 2021, 14, 3284. https://doi.org/10.3390/en14113284

[16] Yang, D., Wang, Y., Pan, R., Chen, R. and Chen, Z. (2018). State-of-health estimation for the lithium-ion battery based on support vector regression, Applied Energy, 227(March), 273–283, http://dx.doi.org/10.1016/j.apenergy.2017.08.096.

[17] Zhang, X., Wang, Y., Liu, C. and Chen, Z. (2018). A novel approach of battery pack state of health estimation using artificial intelligence optimization algorithm, Journal of Power Sources, 376(September 2017), 191–199, https://doi.org/10.1016/j.jpowsour 2017.11.068.

[18] Lin, C., Xing, J. and Tang, A. (2017). Lithium-ion Battery State of Charge/Statebof Health Estimation Using SMO for EVs, Energy Procedia, 105, 4383–4388, http://dx.doi.org/10.1016/j.egypro.2017.03.931.

[19] Zhou, X., Stein, J.L. and Ersal, T. (2017). Battery state of health monitoring by estimation of the number of cyclable Li-ions, Control Engineering Practice, 66(April), 51–63, http://dx.doi.org/10.1016/j.conengprac.2017.05.009.

[20] Salameh, Mohamad et al. “Thermal State of Charge Estimation in Phase Change Composites for Passively Cooled Lithium-Ion Battery Packs.” IEEE Transactions on Industry Applications 54 (2018): 426-436.

[21] Buidin, Thomas Imre Cyrille, and Florin Mariasiu. "Battery thermal management systems: Current status and design approach of cooling technologies." Energies 14.16 (2021): 4879.

[22] Belarbi, Abdelillah Abed, et al. "Experimental investigation on controlled cooling by coupling of thermoelectric and an air impinging jet for CPU." Heat Transfer 50.3 (2021): 2242-2258.

[23] Warner, John T. The handbook of lithium-ion battery pack design: chemistry, components, types and terminology. Elsevier, 2015.

[24] https://en.wikipedia.org/wiki/Baghdad_Battery

[25] Park, J. (2012). Principles and Applications of Lithium Secondary Batteries, Engineering Pro collection, Wiley, https://books.google.com.tr/books?id=papHH-urMVYC.

[26] https://www.istockphoto.com/tr/vekt%C3%B6r/voltaic-pile-first-electrical-battery-by-alessandro-volta-published-1880-gm518507608-90077923

[27] Elizabeth H. Oakes, A to Z of STS Scientists, p. 72, Info base Publishing, 2009 1438109253.

[28] Morus, Iwan Rhys. "Currents from the underworld: electricity and the technology of display in early Victorian England." Isis 84.1 (1993): 50-69.

[29] Ozawa, K. (2009). Lithium Ion Rechargeable Batteries. Wiley-VCH Verlag GmbH&Co. KGaA, Weinheim, Germany.

[30] https://www.helios-h2020project.eu/news/batteries-long-history-powerful-future

[31] A. A. Pesaran, A. Vlahinos, T. Stuart, Cooling and Preheating of Batteries in Hybrid Electric Vehicles, Japanese Soc. Mech. Eng.: The 6th ASME-JSME Therm. Eng. Jt. Conf. (2003) 1-7.

[32] T. Zhang, C. Gao, Q. Gao, G. Wang, M. Liu, Y. Guo, C. Xiao, Y.Y. Yan, Status and development of electric vehicle integrated thermal management from BTM to HVAC, Appl. Therm. Eng. 88 (2015) 328-409.

[33] Z. Rao, S. Wang, a review of power battery thermal energy management, Renew. Sustain. Energy Rev. 15 (2011) 4554-4571.

[34] G-H Kim et al. “Multi-Domain Modeling of Lithium-Ion Batteries Encompassing Multi-Physics in Varied Length Scales”. J. of Electrochemical Soc. 158 (8). A955 A969. 2011.

[35] ANSYS Fluent Battery Module Manual, pages 17-18.

[36] M. Chen and G. A. Rincon-Mora. “Accurate Electrical Battery Model Capable of Predicting Runtime and I-V Performance”. IEEE Trans. On Energy Conversion. Vol. 21. No.2. A154-A161. June 2006.

[37] L. Cai and R.E. White. “Reduction of Model Order Based on Proper Decomposition for Lithium-Ion Battery Simulations”. J. of Electrochemical Soc. 156(3). A154-A161. 2009.

[38] Madani, Seyed Saeed, Maciej Swierczynski, and Søren Knudsen Kær. "Cooling simulation and thermal abuse modeling of lithium-ion batteries using the Newman, Tiedemann, Gu, and Kim (NTGK) model." ECS Transactions 81.1 (2017): 261.

[39] U. S. Kim et al. “Effect of electrode configuration on the thermal behavior of a lithium-polymer battery”. Journal of Power Sources. 180 (2). 909-916. 2008.

[40] K. Smith and C.Y. Wang. “Solid-state Diffusion Limitations on Pulse Operation of a Lithium Ion Cell for Hybrid Electric Vehicles”. Journal of Power Sources. 161. 628-639. 2006.

[41] D. I. Stroe, M. Swierczynski, A. I. Stroe, and S. K. Kær, “Generalized characterization methodology for performance modelling of lithium-ion batteries,” Batteries, vol. 2, no. 4, 2016.

[42] Warner, John T. The handbook of lithium-ion battery pack design: chemistry, components, types and terminology. Elsevier, 2015.

[43] https://en.wikipedia.org/wiki/Baghdad_Battery

[44] https://www.lifepo4-battery.com/Products/CALB-Battery/CALB-L160F100-100Ah.html

CURRICULUM VITAE

PERSONAL INFORMATION

Name - Surname : Recep UYSAL

EDUCATION

Postgraduate

Marmara University – Istanbul, TURKEY (2018 - Still)
School of Institute of Science and Technology-Department of Mechanical Engineering (English)

Undergraduate

Istanbul Technical University – Istanbul, TURKEY (2008-2014)
School of Engineering-Department of Mechanical Engineering (English)

High School

Nazilli Anatolian Teacher High School – Aydın, TURKEY (2004-2008)

SCIENTIFIC WORKS

International Conference Publications:

Uysal R., Yılmaz B., Numerical Analysis and Experimental Verification of Industrial Lithium-Ion Batteries, 1st International Conference on Engineering and Applied Natural Sciences on 10-13 May in 2022. (Oral)